Rapid Chlorophyll *a* Fluorescence Light Response Curves Mechanistically Inform Photosynthesis Modeling[1][OPEN]

Jonathan R. Pleban,[a,2] Carmela R. Guadagno,[b,2,3,4] David S. Mackay,[a] Cynthia Weinig,[b,c,d] and Brent E. Ewers[b,c]

[a]Department of Geography, State University of New York, Buffalo, New York 14260
[b]Department of Botany, University of Wyoming, Laramie, Wyoming 82071
[c]Program in Ecology, University of Wyoming, Laramie, Wyoming 82071
[d]Department of Molecular Biology, University of Wyoming, Laramie, Wyoming 82071

ORCID IDs: 0000-0003-0292-4744 (J.R.P.); 0000-0003-1940-0250 (C.R.G.); 0000-0003-0477-9755 (D.S.M.); 0000-0001-6647-7475 (B.E.E.).

Crop improvement is crucial to ensuring global food security under climate change, and hence there is a pressing need for phenotypic observations that are both high throughput and improve mechanistic understanding of plant responses to environmental cues and limitations. In this study, chlorophyll *a* fluorescence light response curves and gas-exchange observations are combined to test the photosynthetic response to moderate drought in four genotypes of *Brassica rapa*. The quantum yield of PSII (ϕ_{PSII}) is here analyzed as an exponential decline under changing light intensity and soil moisture. Both the maximum ϕ_{PSII} and the rate of ϕ_{PSII} decline across a large range of light intensities (0–1,000 μmol photons m^{-2} s^{-1}; β_{PSII}) are negatively affected by drought. We introduce an alternative photosynthesis model (β_{PSII} model) incorporating parameters from rapid fluorescence response curves. Specifically, the model uses β_{PSII} as an input for estimating the photosynthetic electron transport rate, which agrees well with two existing photosynthesis models (Farquhar-von Caemmerer-Berry and Yin). The β_{PSII} model represents a major improvement in photosynthesis modeling through the integration of high-throughput fluorescence phenotyping data, resulting in gained parameters of high mechanistic value.

Increasing global populations and environmental change require greater mechanistic understanding of plant responses to fluctuating environmental factors along with meaningful phenotyping for tolerance to stress such as drought (Sheffield and Wood, 2008; Jin et al., 2018). Improved phenotyping technologies can also advance our ability to link physiological mechanisms to rapidly improving genetic information. Among the challenges toward this goal is the genetic complexity behind drought tolerance traits of interest to breeders (Holland, 2007; Shi et al., 2009). Hence, model-assisted phenotyping has been advocated to separate complex traits such as quantum yield of photosynthesis, stomatal conductance, and water use efficiency into manageable mechanistic components (Tardieu, 2003). Mechanistic modeling formalizes plant physiology using interconnected mathematical equations, which describe primary biochemical and first-principles biophysical processes. Improving predictive understanding of crop responses to changing environments will require that mechanistic models directly use phenotypic and environmental data to simulate outcomes sensitive enough to capture possible variation in the expressed traits among unknown genotypes. When these requirements are met, mechanistic models can assist in unraveling the genetic architecture underlying the complex quantitative traits of drought physiology (Reymond et al., 2003; Hammer et al., 2006; Chenu et al., 2009).

Although mechanistic models have evolved to capture the expression of complex plant traits in a changing environment, no current model can dependably capture the impact of drought on photosynthesis (Drake et al., 2017). Photosynthesis models focus on those environmental factors considered critical to net assimilation rates (A_n; de Witt, 1966; Farquhar et al., 1980; Patrick et al., 2009; Yin et al., 2009). Observations of A_n and available CO_2 (A/C_i) are combined in mechanistic models, such as the Farquhar, von Caemmerer, and Berry (FvCB) model (Farquhar et al., 1980), to reveal biochemical

[1]This work was supported by the National Science Foundation Plant Genome Research Project (grant nos. IOS–1444571, IOS–1025965, and IOS–1547796), the University at Buffalo Mark Diamond Research Foundation, and the College of Arts and Sciences Dissertation Enhancement Grant.

[2]These authors contributed equally to the article.

[3]Senior author.

[4]Author for contact: cguadagn@uwyo.edu.

The author responsible for distribution of materials integral to the findings presented in this article in accordance with the policy described in the Instructions for Authors (www.plantphysiol.org) is: Carmela Rosaria Guadagno (cguadagn@uwyo.edu).

J.R.P., C.R.G., D.S.M., and B.E.E. contributed to updated model conceptualizations; J.R.P., C.R.G., and D.S.M. contributed to experimental design; C.R.G. and J.R.P. performed experiments; J.R.P. implemented and conducted analysis of all models; C.R.G. and J.R.P. contributed original draft preparation; C.R.G., J.R.P., B.E.E., C.W., and D.S.M. contributed to review and editing.

[OPEN]Articles can be viewed without a subscription.

www.plantphysiol.org/cgi/doi/10.1104/pp.19.00375

mechanisms underpinning photosynthesis. FvCB estimates A_n as limited by two primary factors. First, Rubisco-limited A_n (A_c) is dominated by the response of the maximum rate of carboxylation (V_{cmax}). Second, light-limited A_n (A_J) is constrained by the electron transport rate (ETR) across PSII and PSI, which ultimately produces ATP and NADPH needed for the Calvin carboxylation cycle (Farquhar et al., 1980; Von Caemmerer, 2000). Although the FvCB model captures the phenomenological link between ETR and A_n, it omits mechanistic details of the photosynthetic electron transport chain (Horton et al., 1994; Allen and Pfannschmidt, 2000; Laisk et al., 2002; Yin et al., 2004). Whereas the conceptual power of a reduced complexity model (FvCB) yields crucial insights under nonstressed conditions, it lacks additional mechanistic detail for plants exposed to environmental stress (Urban et al., 2017).

Drought stress impacts both A_c and A_J via interactive mechanisms (Flexas and Medrano, 2002; Bota et al., 2004; Fini et al., 2012). The initial response to water stress is often a decline in stomatal conductance (g_s), which impacts CO_2 availability for photosynthesis (Medrano et al., 2002; Grassi and Magnani, 2005). Additional CO_2 constraints on A_c are possible via mesophyll conductance (g_m), limiting CO_2 at the site of carboxylation (Flexas et al., 2002, 2018; Niinemets et al., 2009; Pons et al., 2009). Prolonged CO_2 limitation can result in overreduction of the photosynthetic electron transport chain (Miller et al., 2010), triggering the production of reactive oxygen species at different sites of the photosynthetic pathway with the potential for photooxidative damage (Krieger-Liszkay et al., 2008; Miller et al., 2010; Sharma et al., 2012). PSII is highly susceptible to oxidative stress, and a variety of mechanisms, collectively called photoprotection, preserve it from irreversible photodamage that causes sustained declines in the overall efficiency of PSII (Murata et al., 2007; Takahashi and Badger, 2011). Heat energy dissipation, state transitions, augmented PSI energy utilization, and changes in leaf absorbance using alternate pigments or chloroplast avoidance are all known mechanisms of photoprotection (Müller et al., 2001; Kasahara et al., 2002; Takahashi and Badger, 2011).

Photosynthesis models must now progress to reflect these stress-induced mechanisms while using high-throughput phenotyping data, including noninvasive measures of leaf spectral reflectance, absorbance, and chlorophyll *a* fluorescence (Cruz et al., 2016; Kuhlgert et al., 2016; Silva-Perez et al., 2018). Fast and informative techniques provide fine temporal resolution of mechanistic responses to external stressors from mild to lethal stress (Guadagno et al., 2017), which are necessary to improve predictive understanding of photosynthesis responses to drought.

In particular, pulse amplitude modulated (PAM) chlorophyll *a* fluorescence analysis quantifies PSII activity in response to observed photosynthetically active radiation (Q) and is informative of the status of the photosynthetic electron transport (Maxwell and Johnson, 2000; Kramer et al., 2004a; Baker, 2008). PAM measurements, using the signal of the excitation energy reemitted by the chlorophyll *a* molecule as fluorescence, are used to define the fate of the absorbed light in the leaf and are currently one of the fastest and most reliable phenotyping tools in photosynthetic measurements (Filek et al., 2015; Gullì et al., 2015; Flood et al., 2016; Guadagno et al., 2017; Gómez et al., 2018). The operating efficiency of PSII (ϕ_{PSII}) is a fluorescence parameter calculated from the relative difference in light conditions between the steady-state fluorescence (F_s) and the maximum fluorescence emitted after a saturating flash that closes (reduces) all PSII reaction centers [F_m'; i.e. $\phi_{PSII} = (F_m' - F_s)/F_m'$; Genty et al., 1989]. A large fraction of the excitation energy not used in PSII photochemistry or reemitted as fluorescence is dissipated as heat via regulated (e.g. nonphotochemical quenching [NPQ]) and nonregulated energy dissipation (e.g. ϕ_{NO}) mechanisms (Müller et al., 2001; Kramer et al., 2004a). Recently, the original derivation of NPQ has been extended, allowing for high-throughput estimates of quantum yield NPQ (ϕ_{NPQt}; Tietz et al., 2017). ϕ_{NPQt} can be measured in a few seconds, allowing for high-throughput and field applications, and its calculation does not require full relaxation of quenching processes as for the classic NPQ parameter. The combination of fluorescence observations with leaf gas-exchange data has been shown as a powerful way to inform and test models of photosynthesis (Laisk et al., 2002; Yin et al., 2009; Bellasio et al., 2016).

Alternative models of photosynthetic electron transport have been developed using an increasing number of mechanistic details of the Z-scheme for the electron transport (Fig. 1). Within chloroplasts, photosynthetic electron transport occurs across the thylakoid membranes (Fig. 1A), where a hydrogen ion gradient builds up upon the transfer of excited e^- to ultimately produce ATP and NADPH, which are used as substrates in the Calvin cycle. Figure 1B summarizes the ETR derivation of the FvCB model. This model assumes that the electron flow is entirely linear (LEF) from PSII to $NADP^+$ reduction, with the CO_2 fixation rate from the A/C_i response used to parametrize the maximum ETR (J_{max}). Data from the linear portion of a light response curve can be used to parameterize quantum yield on a $\Delta CO_2/\Delta Q$ basis (ϕ_{CO2}; Fig. 1B, inset graph). Although the significance of the correlation between the quantum yield of assimilation and the PSII quantum yield has been previously studied (Oberhuber and Edwards, 1993; Pietrini and Massacci, 1998; Singsaas et al., 2001), to the best of our knowledge, the effect of drought on its linearity is still unclear. The FvCB model has been recently implemented to include proportional changes between ETR and A_n using observations of A_n and ϕ_{PSII} under low-light conditions ($Q < 200$ μmol photons m^{-2} s^{-1}) to estimate ETR and A_J (Fig. 1C; Yin et al., 2004, 2009; Bellasio et al., 2016). Quantum yield is estimated on a $\Delta e^-/\Delta Q$ basis using the linear portion of the ϕ_{PSII} light response (Fig. 1C, top inset graph), but the use of only low-light conditions to characterize PSII quantum

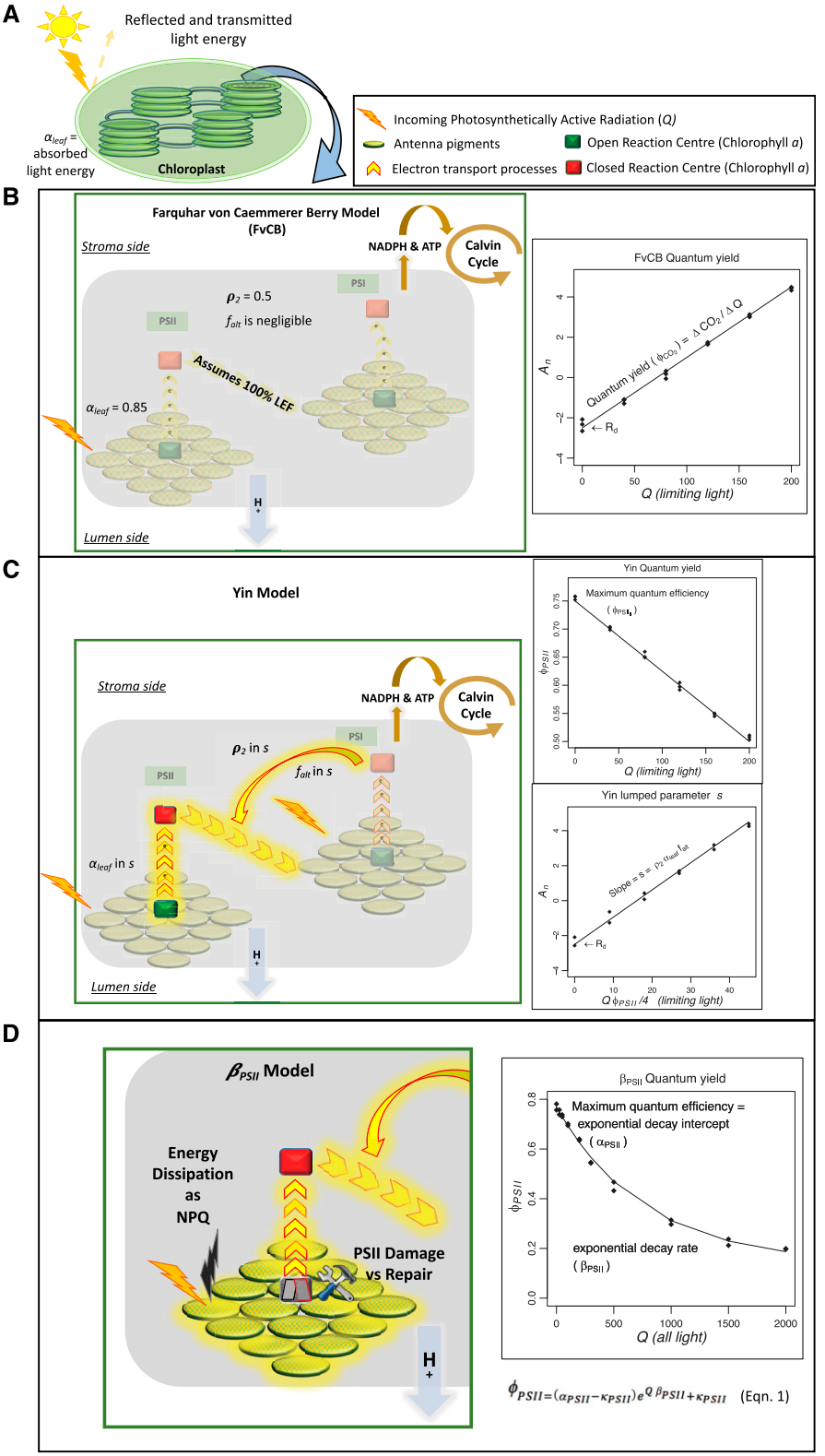

Figure 1. Simplified illustration of the light reactions of photosynthesis representing how three conceptual models account for the photosynthetic electron transport. A, Upon light energy absorption, energy in the form of excited electrons (e^-) is transferred from light-harvesting antennae to the reaction centers of PSI and PSII in the chloroplastic thylakoid membranes. This energy transport has been described as a Z-scheme (Hill and Bendall, 1960) whereby e^- from PSII produce a transmembrane H^+ gradient (used for ATP production) while e^- downstream of PSI produce NADPH; both ATP and NADPH are then used for Calvin cycle CO_2 fixation.

yield is limiting. In the Yin model, a lumped parameter, s, is estimated to account for the energy partitioning between photosystems (ρ_2), leaf absorbance in the antenna complex (α_{leaf}), and the potential use of electron pathways other than LEF (f_{alt}). However, neither FvCB nor the Yin model explicitly addresses the influence of environmental stress on ETR and A_n, and they are not well equipped to capture the A_J responses of the PSII antenna complex to stressors (Govindjee, 2002; Asada, 2006; Murata et al., 2007; Urban et al., 2017).

Here, we introduce an alternative approach (β_{PSII} model) that considers PSII activity across a wide range of light conditions and that can better accommodate the role of stress-related mechanisms (Fig. 1D). We observe that data from the ϕ_{PSII}/Q response can be modeled as an exponential decline (Fig. 1D, inset graph). This new parameter as the rate of decline (β_{PSII}) can be used to calculate ETR, A_J, and A_n under stress conditions such as drought. Using a more complete characterization of quantum yield via the ϕ_{PSII} light response, the β_{PSII} model approach accommodates mechanisms of photoprotection including NPQ, chloroplast avoidance, and pigment alterations as well as PSII damage relative to repair (Fig. 1D). Our integration of the ϕ_{PSII} decline provides a link between gas conductance-based limitations on A_c and photoprotective limitations impacting A_J, representing a further step in the mechanistic understanding of the electron transport under stress (incremental yellow shadow in Fig. 1). All model parameters (observed and predicted) for the FvCB, Yin, and β_{PSII} models are compared in Table 1, whereas Table 2 describes the equations used in the three photosynthesis models.

We tested the β_{PSII} approach in an effort to analyze physiological responses of A_n under different soil moisture conditions from full watering to moderate drought in the species *Brassica rapa* (Supplemental Figs. S1 and S2). High intraspecific physiological diversity with respect to complex quantitative traits such as A_n and water use efficiency has previously been shown for *Brassica* species (Edwards et al., 2011, 2012; Franks, 2011; Baker et al., 2015), making it a perfect model to investigate photosynthesis phenotyping tools. Specifically, we tested a turnip crop type (*VT*), a cultivated oilseed (*R500*), and two experimental genotypes (recombinant inbred lines [RILs]) developed from a cross between a rapid-cycling genotype (*Imb211*) and an oilseed crop (*R500*), thus ensuring a broad range of both photosynthetic and biomass allocation diversity (Edwards et al., 2011; Yarkhunova et al., 2016; Pleban et al., 2018).

We developed a ϕ_{PSII} light response curve using a three-parameter exponential function,

$$\phi_{PSII} = (\alpha_{PSII} - \kappa_{PSII})e^{Q\beta_{PSII}} + \kappa_{PSII} \quad (1)$$

where the exponential rate of decline for ϕ_{PSII} (β_{PSII}) under increasing light (Q) and the intercept of ϕ_{PSII} as Q approaches zero (α_{PSII}) are used to model the responses. Importantly, α_{PSII} derives from measurements taken in light conditions and is different that the classic F_v/F_m parameter derived from dark-adapted measurements (Table 1). The κ_{PSII} term represents a non-zero minimum of ϕ_{PSII} as Q approaches ∞. To evaluate potential differences in photoprotection strategies due to ETR, we validated the ϕ_{PSII} light response parameters (β_{PSII} and α_{PSII}) at different soil moisture conditions. Then, we incorporated these parameters in an alternative photosynthesis model that directly incorporates ϕ_{PSII} light response traits into the estimation of ETR, and we assessed how the derived parameters relate to known traits, including V_{cmax} and g_m.

Using rapid measurements with high mechanistic significance, our approach innovatively connects high-throughput phenotyping and biophysical modeling to better predict plant photoprotective strategies. Gained knowledge will help to clarify the complexity of photosynthetic traits, such as drought tolerance, thus improving breeding and management strategies toward more drought-resistant crops with increased final yield.

RESULTS

Establishing Drought Treatments

After sowing, plants were immediately randomized and put into different treatment groups (Supplemental

Figure 1. (*Continued.*)
For modeling applications (inset graphs of B, C, and D), photosynthetic quantum yield describes how light energy relates to CO_2 fixation (Genty et al., 1989; Martre et al., 2015) and assumptions are made about the processes of electron transfer more or less obscuring (gray boxes in B, C, and D) the actual physiological mechanisms. B, In the traditional FvCB conceptualization, quantum yield is calculated on a photon-to-CO_2 basis (ϕ_{CO2}; inset graph). Here, ETR processes are ignored, assuming 100% LEF from PSII to NADPH production, leaf absorbance (α_{leaf}) is fixed (0.85), and an implicit 50:50 fractionalization of Q exists between PSII and PSI (ρ_2). C, The Yin conceptualization improved the use of PSII physiology by calculating quantum yield on a photon-to-e$^-$ basis, using the relationship between ϕ_{PSII} and Q under light-limiting conditions (ϕ_{PSII_ll}; top inset graph). Yin also used a lumped s parameter defined by the slope of a linear regression of A_n against $(Q\,\phi_{PSII})/4$ using light < 200 μmol m^{-2} s^{-1}, where 4 is the number of protons needed to synthesize one ATP. This regression was used to calibrate for three factors, the unknown fraction of nonlinear electron flow around PSI (f_{alt}), α_{leaf}, and ρ_2 (collectively s; bottom inset graph). D, Our alternative β_{PSII} conceptualization captures the behavior of energy transfer from the antennae complex to the PSII reaction complex. Here, quantum yield is modeled using an exponential decay function (Eq. 1) across all relevant Q conditions, on a photon-to-e$^-$ basis, providing estimates of both maximum light-acclimated quantum yield (α_{PSII}) and the decay rate in ϕ_{PSII} under increasing Q (β_{PSII}; inset graph). The β_{PSII} model maintains the use of the s parameter to address f_{alt}, α_{leaf}, and ρ_2. Implementations of modeling photosynthetic electron transport in the Yin and β_{PSII} approaches are represented as incrementing highlighted yellow in C and D.

Table 1. *List of abbreviations used for models (observations, predictions, and parameters)*

Abbreviation	Definition	Units
A_n	CO_2 assimilation rate observed	μmol m^{-2} s^{-1}
C_i	Intercellular CO_2 partial pressure observed	Pa
T_{leaf}	Leaf temperature observed	°C
g_s	Conductance to CO_2 from atmosphere to intercellular space observed	μmol m^{-2} s^{-1}
O	Ambient O_2 (assumed 21% atmosphere)	Pa
Q	Photosynthetically active radiation observed	μmol m^{-2} s^{-1}
ϕ_{PSII}	Operating efficiency of PSII ($F_m' - F_s'/F_m'$) observed	e^- $photon^{-1}$
A_c	Predicted Rubisco limited rate of CO_2 assimilation	μmol m^{-2} s^{-1}
A_j	Predicted electron transport limited rate of CO_2 assimilation	μmol m^{-2} s^{-1}
J_m	Predicted rate of electron transport following FvCB	μmol m^{-2} s^{-1}
J_f	Predicted rate of electron transport following Yin	μmol m^{-2} s^{-1}
J_l	Predicted rate of electron transport following beta decay model	μmol m^{-2} s^{-1}
R	Universal gas constant (8.314 J K^{-1} mol^{-1})	J K^{-1} mol^{-1}
α_{leaf}	Absorptance of leaf photosynthetic pigments	%
ρ_2	Partitioning of energy between PSII and PSI	%
f_{alt}	Fraction of electron not using LEF ($1 - f_{pseudo(b)}/(1 - f_{cyc})$ in Yin et al. (2009)	%
s	Lumped parameter (ρ_2 α_{leaf} f_{alt}; Yin et al., 2009)	%
Γ^*25	CO_2 photocompensation point (standardized to 25°C)	Pa
K_{c25}	Michaelis-Menten constant for Rubisco for CO_2 (standardized to 25°C)	Pa
K_{o25}	Michaelis-Menten constant for Rubisco for O_2 (standardized to 25°C)	kPa
Ei's (K_c, K_o, R_d, V_{cmax}, Γ^*, J_{max}, g_m)	Activation energy used in Arrhenius function	KJ mol^{-1}
R_{d25}	Respiration rate in the dark (standardized to 25°C)	μmol m^{-2} s^{-1}
g_{m25}	Mesophyll conductance (standardized to 25°C)	μmol m^{-2} s^{-1} Pa^{-1}
V_{cmax25}	Maximum rate of carboxylation (standardized to 25°C)	μmol m^{-2} s^{-1}
J_{max25}	Maximum rate of electron transport (standardized to 25°C)	μmol m^{-2} s^{-1}
ϕ_{CO2}	Quantum yield of CO_2 using Equation 2.6	mol CO_2 mol^{-1} photon
θ_J	Curvature factor on electron transport rate predictions J_m and J_f	unitless
ϕ_{PSII_ll}	Maximum quantum efficiency following Yin using Equation 2.6	mol e^- mol^{-1} photon
β_{PSII}	Decay rate in ϕ_{PSII} under increasing Q using Equation 1	Q^{-1}
α_{PSII}	Modeled ϕ_{PSII} as Q approaches zero using Equation 1	unitless
κ_{PSII}	Modeled ϕ_{PSII} as Q approaches ∞ using Equation 1	unitless

Fig. S1). On experimental day 0 (28 d after sowing), drought was applied via complete water withholding for the droughted cohort. Control pots (well watered [WW]) were watered daily throughout the experiment, and WW plants were measured on experimental days 1, 4, 5, 6, and 9. Droughted plants were assigned to three different groups, and replicate plants were observed on experimental days 4 to 7 (treatment group D1), 9 to 12 (treatment group D2), and 15 (treatment group D3). On experimental day 9, water was reapplied to a subset of droughted plants (R1), and they were observed on experimental days 9 to 12. On experimental day 15, a second subset of droughted plants (R2) was rewatered and observed 6 h after rewatering. Finally, on day 16, the last subset of droughted plants was rewatered and assessed at 30 h after rewatering (R3). For each experimental day, volumetric soil water content (VWC) was measured across all cohorts of plants for the duration of the experiment (Supplemental Fig. S2).

Impact of Drought on Leaf Traits and Genotypic Difference

The progressive drought and recovery (Supplemental Fig. S1) application inevitably impacted the photosynthetic performance of all genotypes. Table 3 summarizes 14 photosynthetic leaf traits assessed on three different experimental days for each *B. rapa* genotype. As expected, D1 plants were the least impacted by water scarcity for the measured physiological traits. However, early signs of drought stress were already detected. g_s was reduced in D1 plants of all genotypes by a mean of 0.16 ± 0.1 mmol m^{-2} s^{-1}, with the biggest decline for *R500* (0.29 mmol m^{-2} s^{-1}). In *VT*, the electrochromic shift (*ECSt*; Δ absorbance 530 nm), which reflects the transthylakoidal ΔH^+ gradient, at 300 and 1,000 μmol photon m^{-2} s^{-1}, increased in D1 plants relative to WW plants. More sustained drought (D2 and D3 plants) results in pronounced changes across all genotypes (Table 3). g_s showed further reduction in all genotypes but *r46* in D3 plants. LEF was decreased across genotypes, with *R500* showing the greatest loss at both 300 and 1,000 μmol photon m^{-2} s^{-1}.ϕ_{NPQt} and *ECSt* at both 300 and 1,000 μmol m^{-2} s^{-1} increased overall in D3 plants. Pigments content as SPAD at 530 nm units and relative chlorophyll content increased in all four genotypes of the D3 cohort. The changes in *ECSt*, LEF, and SPAD are reflected in a decreased lumped *s* parameter in D3 plants, which accounts for potential changes in f_{alt}, ρ_2, and α_{leaf} (Supplemental Fig. S3). These results validate the robustness of high-throughput measurements of fluorescence to pick up early signs of drought stress. The drought treatments applied here can be

Table 2. *List of equations used in three photosynthesis models (FvCB, Yin, and β_{PSII} decay)*

Equation No.	Equation	Description
2.1	$A_n = \begin{cases} A_c \text{ if } C_i < C_{crit} \\ A_j \text{ if } C_i > C_{crit} \end{cases}$	A_n depending on two limiting factors and the critical C_i (C_{crit})
2.2	$A_i = \frac{-b+\sqrt{b^2-4ac}}{2a}$	General quadratic form for solving A_c, A_j, J_m, and J_f
2.3	$a = \frac{-1}{g_m}$ $b = \frac{V_{cmax} - R_d}{g_m} + C_i + K_c\left(\frac{1+O}{K_o}\right)$ $c = R_d\left(C_i + K_c\left(\frac{1+O}{K_o}\right)\right)$	Quadratic roots using intercellular CO_2 (C_i) and a g_m term for describing A_c
2.4	$a = \frac{-1}{g_m}$ $b = \frac{\frac{J_i}{4} - R_d}{g_m} + C_i + 2\Gamma^*$ $c = R_d(C_i + 2\Gamma^*) - \frac{J_i}{4}(C_i - \Gamma^*)$	Quadratic roots for A_j using J_m, J_f, or J_I
2.5	$Q_{abs} = Q\alpha_{leaf}$ $a = \theta_J$ $b = -(Q_{abs}\phi_{CO_2}) - J_{max}$ $c = Q_{abs}\phi_{CO_2}J_{max}$	Quadratic roots for whole-chain ETR (J_m) as described by Von Caemmerer (2000) assumes $\alpha_{leaf} = 0.85$
2.6	$a = \theta_J$ $b = -(Qs\phi_{II_{ll}}) - J_{max}$ $c = Qs\phi_{II_{ll}}J_{max}$	Quadratic roots for combined gas-exchange and chlorophyll fluorescence ETR (J_f) as described by Yin et al. (2009), $s = \alpha_{leaf} f\, f_{alt}$
2.7	$J_I = \phi_{pred}sQ$	β_{PSII} model for full ϕ_{PSII} versus Q derivation of ETR (J_I) using Equation 1 to predict ϕ_{II} from decay with Q

considered as mild to moderate for *B. rapa*, with an overall recorded VWC never lower than 3% and plants still capable of recovery upon rewatering for all genotypes (Supplemental Fig. S1). Changes in physiological traits reflect the expected behavior of the four genotypes under drought (Edwards et al., 2011, 2012; Baker et al., 2015; Greenham et al., 2017). Genotypes with high biomass accumulation (*R500*, *r301*, and *VT*) were more impacted at an earlier stage by changes in soil moisture, whereas the small, highly water use-efficient *r46* was able to tolerate drought and maintain a stable level of gas exchange despite the decreased LEF. These genotypic differences in drought behavior were confirmed when looking at the onset of *NPQt* at increased LEF (Supplemental Fig. S4), where *R500* and *VT* showed earlier changes in *NPQt* values already at lower LEF in comparison with the inbred lines *r46* and *r301*.

Analysis of Rapid Light Response Curves of Fluorescence

Rapid chlorophyll *a* fluorescence light response curves were taken on 119 replicate leaves during six different experimental days, with each genotype × treatment replicated one to seven times (mean replication rate of 3.3; Supplemental Fig. S1). The variation in sample size was due to time constraints and destructive measurements occurring during the experiment. First, the rapid light response curves for all genotypes and treatments were pooled together with the mean of observed ϕ_{PSII} at each Q estimated using the median value of the posterior distributions of the parameter from Equation 1. The decline was then fitted with an exponential model for each genotype and treatment (Fig. 2). All genotypes show a decline in ϕ_{PSII} under drought, more pronounced after 15 d (D3), but all plants recovered to prestressed values after rewatering (R1, R2, and R3). The partial increase of ϕ_{PSII} can be found in the rapid leaf development of the utilized genotypes, typical of the Brassicaceae. Since the youngest fully developed leaf was utilized at each measuring point, leaf growth and display changed over the course of 15 d, causing different leaf angles, changes in the photosynthetic complex stoichiometry, and different responses to incoming radiation and absorbance. Then, to utilize a more rigorous and probabilistic approach to signify differences (Kruschke, 2014), we used the 95% posterior high-density intervals (HDIs) as a Bayesian probabilistic estimator of difference. Figure 3 summarizes the changes in β_{PSII} and α_{PSII}, estimated following Equation 1, at varying VWC. Genotypes *VT* and *r301* showed credible interval differences at 95% HDI in β_{PSII} for D2 and D3

Table 3. *Genotype × treatment trait estimates*

Modeled traits show median of posterior distribution (95% credible interval range), while observed traits show mean values (SD). Boldface indicates significance relative to well-watered conditions at $P < 0.05$ or for 95% confidence interval (CI). HDI interval difference not intersecting with zero was used to describe a credible trait variance (A_{max} and s).

Trait	Treatment	*r301*	*r46*	*R500*	*VT*
A_{max}	Well watered	27.70 (25.47, 30.26)	17.12 (14.99, 19.57)	25.42 (22.86, 28.13)	18.25 (15.94, 20.64)
(μmol m^{-2} s^{-1})	Early drought	28.70 (26.02, 31.22)	14.54 (12.73, 16.43)	25.62 (23.33, 27.74)	14.71 (12.91, 16.45)
(95% CI range)	Late drought	**9.70 (7.63, 11.76)**	**8.75 (6.65, 10.71)**	**4.75 (2.17, 7.21)**	**3.30 (−0.74, 6.83)**
s	Well watered	0.33 (0.3, 0.37)	0.29 (0.25, 0.32)	0.32 (0.29, 0.34)	0.31 (0.27, 0.35)
unitless	Early drought	0.36 (0.33, 0.38)	0.28 (0.25, 0.31)	0.32 (0.3, 0.34)	0.29 (0.25, 0.32)
(95% CI range)	Late drought	**0.16 (0.12, 0.2)**	**0.19 (0.15, 0.22)**	0.26 (0.02, 0.53)	**0.11 (0.05, 0.17)**
ESCt_300 × 1000	Well watered	1.7 (0.35)	1.7 (0.34)	1.4 (0.32)	1.2 (0.42)
Δ absorbance 530 nm	Early drought	**1.4 (0.10)**	1.7 (0.49)	1.8 (0.48)	1.9 (0.32)
(SD)	Late drought	**3.0 (0.44)**	2.4 (0.13)	**2.7 (0.24)**	**2.7 (0.21)**
ESCt_1000 × 1,000	Well watered	2.7 (0.15)	2.6 (0.27)	2.5 (0.29)	1.9 (0.78)
Δ absorbance 530 nm	Early drought	2.5 (0.18)	2.3 (0.35)	2.3 (0.65)	2.4 (0.22)
(SD)	Late drought	**3.7 (0.43)**	**3.1 (0.27)**	3.6 (0.57)	**3.7 (0.07)**
LEF_300	Well watered	61.07 (2.90)	57.37 (0.26)	70.25 (4.43)	64.06 (3.39)
(μmol m^{-2} s^{-1})	Early drought	68.72 (0.18	57.46 (7.59)	63.27 (4.34)	61.23 (3.05
(SD)	Late drought	**34.48 (11.38)**	**43.06 (7.59)**	**36.21 (5.70)**	**42.39 (1.53)**
LEF_1000	Well watered	93.00 (6.78)	79.14 (8.03)	106.17 (6.76)	92.48 (7.64)
(μmol m^{-2} s^{-1})	Early drought	105.18 (0.30)	76.93 (2.65)	98.07 (17.36)	88.93 (9.63)
(SD)	Late drought	**49.22 (13.29)**	**54.62 (10.92)**	**51.74 (8.27)**	**59.93 (3.61)**
φ_{NPQt_300}	Well watered	0.31 (0.03)	0.33 (0.04)	0.21 (0.03)	0.24 (0.04)
(%)	Early drought	0.24 (0.02)	0.32 (0.01)	0.27 (0.06)	0.28 (0.03)
(SD)	Late drought	**0.55 (0.05)**	**0.49 (0.07)**	**0.52 (0.08)**	**0.49 (0.03)**
φ_{NPQt_1000}	Well watered	0.64 (0.02)	0.66 (0.02)	0.57 (0.03)	0.59 (0.04)
(%)	Early drought	0.6 (0.01)	0.67 (0.01)	0.60 (0.06)	0.62 (0.03)
(SD)	Late drought	**0.73 (0.01)**	**0.73 (0.02)**	**0.69 (0.05)**	**0.69 (0.01)**
φ_{NO_300}	Well watered	0.21 (0.019)	0.22 (0.009)	0.24 (0.011)	0.25 (0.028)
(%)	Early drought	0.22 (0.018)	0.23 (0.01)	0.23 (0.032)	0.24 (0.011)
(SD)	Late drought	0.18 (0.045)	0.17 (0.015)	0.20 (0.036)	0.18 (0.019)
φ_{NO_1000}	Well watered	0.15 (0.022)	0.15 (0.006)	0.18 (0.018)	0.20 (0.029)
(%)	Early drought	0.15 (0.005)	0.15 (0.011)	0.17 (0.021)	0.17 (0.008)
(SD)	Late drought	0.15 (0.026)	**0.14 (0.007)**	0.19 (0.035)	**0.16 (0.005)**
SPAD 530	Well watered	58.66 (3.93)	52.42 (6.57)	58.53 (5.8)	41.54 (8.2)
	Early drought	53.06 (7.57)	45.61 (7.39)	56.86 (17.02)	43.19 (9.4)
(SD)	Late drought	98.91 (10.11)	72.59 (11.91)	102.86 (8.66)	84.86 (27.68)
gs	Well watered	0.48 (0.07)	0.21 (0.06)	0.44 (0.12)	0.23 (0.11)
(mmol m^{-2} s^{-1})	Early drought	**0.30 (0.15)**	**0.17 (0.07)**	**0.15 (0.15)**	**0.09 (0.11)**
(SD)	Late drought	**0.19 (0.14)**	**0.17 (0.12)**	**0.04 (0.06)**	**0.06 (0.06)**
Leaf temperature	Well watered	−1.2 (1.57)	−0.68 (1.02)	−0.58 (1.19)	−1.03 (0.94)
Differential (°C)	Early drought	−0.17 (0.81)	0.51 (1.32)	0.45 (1.48)	**1.76 (0.7)**
(SD)	Late drought	−0.1 (1.41)	0.53 (0.57)	0.33 (0.24)	−0.24 (0.35)
Relative	Well watered	45.75 (3.58)	42.46 (5.91)	45.72 (3.03)	29.57 (10.98)
Chlorophyll	Early drought	47.13 (3.18)	38.12 (2.41)	41.29 (14.02)	39.00 (4.99)
(SD)	Late drought	**73.52 (2.04)**	**56.82 (5.37)**	**77.85 (3.67)**	**67.44 (10.18)**

relative to the WW treatment, whereas *r46* and *R500* showed a credible interval difference (95% HDI) only for D3 relative to the WW treatment (Fig. 3, A–D).

All genotypes demonstrated similar recovery patterns in β_{PSII}, with credible differences at 95% HDI for the R2 and R3 treatments relative to D3. For R plants, a less negative β_{PSII} was observed at 30 h after rewatering (R3) with respect to the 6-h period (R2), demonstrating ongoing recovery during that time period. Figure 3, E to H, displays the change of slope in ϕ_{PSII} as Q approaches zero, α_{PSII}, with 95% posterior HDI. *r301*, *R500*, and *VT* all show credible interval differences at 95% HDI in α_{PSII} for D3 relative to WW treatment, whereas *r46* remains stable in α_{PSII}. The α_{PSII} parameter shows a recovery response similar to β_{PSII}, with *r301*, *R500*, and *VT* all showing credible interval differences at 95% HDI for the R3 treatment with respect to prestressed values.

Comparison of Photosynthesis Models

All three photosynthesis models (FvCB, Yin, and β_{PSII}) performed well across genotypes and treatments when comparing observations of leaf gas exchange with simulated results, using the medians of the posterior (i.e. a more rigorous Bayesian estimator that incorporates

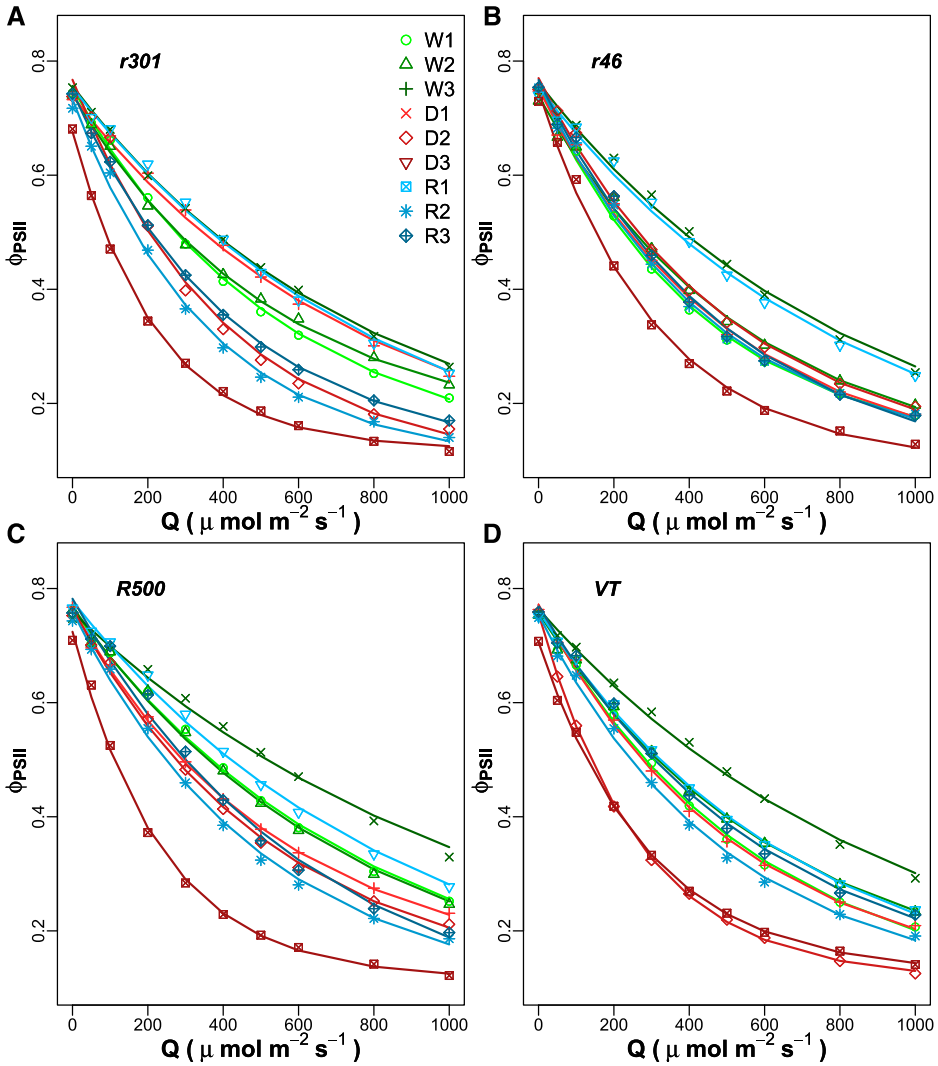

Figure 2. ϕ_{PSII} across photosynthetically active radiation (Q) of 0 to 1,000 μmol photons m^{-2} s^{-1} for four *B. rapa* genotypes. Observations of *r301* (A), *r46* (B), *R500* (C), and *VT* (D) occurred over a range of water regimes from well-watered (W1, W2, and W3) to increasing drought (D1, D2, and D3) conditions and different levels of rewatering (R1, R2, and R3). Points are mean values of replicates (n curves = 119, average n curves per replicate = 3.3), and fitted lines use median posterior estimates of a three-parameter exponential decline model (Eq. 1) by genotype × treatment.

uncertainty in both measurements and models; Kruschke, 2014; McElreath, 2016) parameter distributions. For the β_{PSII} model, a comparison of simulated A_n versus observed A_n from light response and A/C_i curves results in $0.66 < R < 0.98$ across genotypes and treatments (Supplemental Fig. S5).

The β_{PSII} parameter, describing the slope of decline of ϕ_{PSII} versus Q, was integrated into the ETR derivation for estimating light-limited photosynthesis, A_J, and the updated ETR description was compared with both the FvCB and Yin photosynthesis models. To quantitatively evaluate the alternate modeling approaches estimating ETR, posterior parameter distributions were compared between the FvCB, Yin, and β_{PSII} decline models (Figs. 4 and 5). The correlation (R) of the medians of these posterior distributions was chosen to evaluate the strength and direction of a linear relationship among alternative parameterizations. For the parameter V_{cmax}, all models showed close agreement in estimates, with R values of 0.97 to 0.98 (Fig. 4, A–C). For g_m, the R value between the FvCB model and the β_{PSII} model was 0.9, between the Yin model and the β_{PSII} model it was 0.9, and between the FvCB model and the Yin model it was 0.99 (Fig. 4, D–F). Additional posterior parameters not common to all three models were compared with factors with similar biophysical meaning, such as quantum yield terms (ϕ_{CO2}, ϕ_{2II}, and α_{PSII}; Fig. 5, A–C). Agreement between the quantum yield terms is particularly strong between ϕ_{2II} (Yin model) and α_{PSII} (β_{PSII} model; Fig. 5B). The κ_{PSII} estimates show little correlation with J_{max} in the FvCB or Yin model (Fig. 5, D and E), whereas J_{max} estimates in FvCB and Yin are highly correlated. The Yin model and the β_{PSII} model were highly correlated in the lumped s parameter ($R = 0.83$). The convexity factor, θ, used in the FvCB and Yin models shows a correlation of 0.57, with the Yin estimates closer to the maximum of 1. Finally, a comparison was made between β_{PSII} as described in Equation 1 and the V_{cmax} and J_{max} estimates from the FvCB and Yin models. β_{PSII} showed an R value of 0.81 with V_{cmax} as described by the FvCB model and 0.83 with V_{cmax} as described by Yin. β_{PSII} showed $R = 0.69$ with J_{max} estimates of the FvCB model and $R = 0.68$ with Yin (Supplemental Fig. S6).

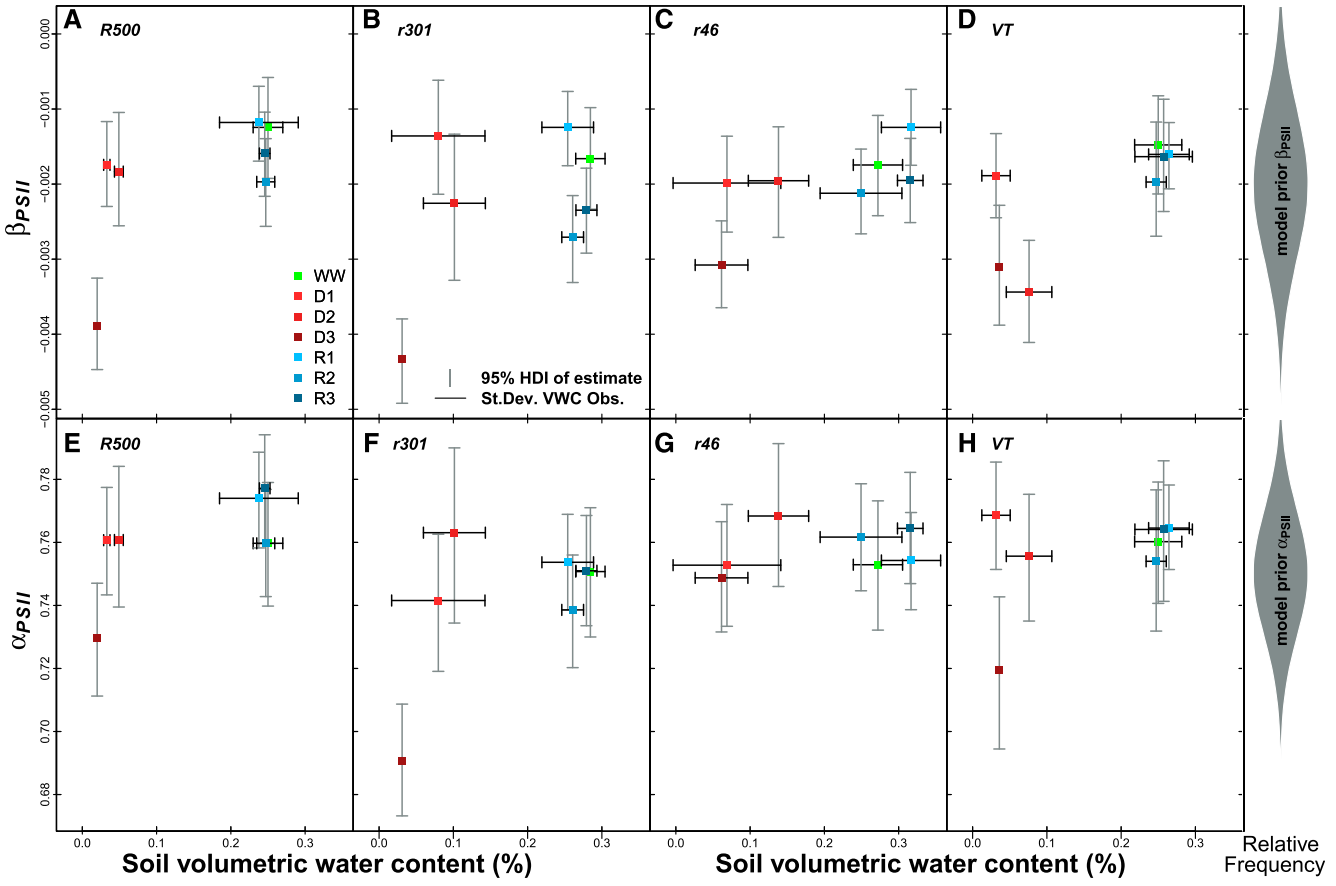

Figure 3. PSII dynamics in response to different water regimes. Decline rate in ϕ_{PSII} under increasing light intensity (β_{PSII} [Q^{-1}]; A–D) and maximum light-acclimated PSII efficiency (α_{PSII}; E–H) are shown for the four *B. rapa* genotypes *R500* (A and E), *r301* (B and F), *r46* (C and G), and *VT* (D and H) over a range of water regimes, as defined in Figure 2, described by VWC. Points represent median posterior estimates of β_{PSII} and α_{PSII} from a three-parameter exponential decline model (Eq. 1; β_{PSII} and α_{PSII} are derived from n curves = 119, average n curves per replicate = 3.3), vertical bars are 95% high-density intervals of posterior estimates, and horizontal bars are SD values on observations of VWC (n = 153, average n per replicate = 4.25). At right are Bayesian prior distributions of β_{PSII} and α_{PSII}.

Comparison of High- and Low-Throughput Fluorescence Measurements

Full gas-exchange light response curves coupled with fluorescence were taken on 34 leaves on four experimental days with each genotype × treatment replicated one to four times (mean replication rate of 2.3 ± 0.9; Supplemental Fig. S1). The variation in sample size was once again due to time constraints and destructive measurements occurring during the experiment. Specifically, the assessment of gas-exchange light response curves was done at experimental days 1 and 6 for WW plants, at days 5 and 7 for D1 plants, and at days 9 and 13 for D2 plants. Rewatered plants in the cohort R2 were observed at experimental day 10 (Supplemental Fig. S1). The assessment of rapid ϕ_{PSII} versus Q curves was done at experimental days 1, 5, and 9 for WW plants, at day 5 for D1 plants, at days 9 and 12 for D2 plants, and at day 13 for D3 plants. Rewatered plants had rapid ϕ_{PSII} versus Q observations for cohort R1 on experimental day 9, for cohort R2 on experimental day 13 (6 h after watering was restored), and for cohort R3 on experimental day 14 (30 h after watering was restored). The comparable posterior parameter estimates were matched with posterior parameter estimates from classic gas-exchange light response curves following Equation 1 and shown in Supplemental Figure S7. The median posterior estimates of β_{PSII} show an R value of 0.72, whereas median posterior estimates of α_{PSII} show R = 0.67 (Supplemental Fig. S7, A and C). Next, the correlation between the posterior estimates for both β_{PSII} and α_{PSII} derived using the full β_{PSII} photosynthesis model and the rapid fluorescence curves was tested (Supplemental Fig. S7, B and D). The full β_{PSII} photosynthesis model utilizes coupled gas-exchange and fluorescence observations from a low-throughput infrared gas analyzer (LiCOR 6400XT), whereas the rapid fluorescence curves of ϕ_{PSII} versus Q curves are obtained using the high-throughput spectrophotometer MultispeQ. Despite the different times of collection, the two methods agree, with correlations of 0.66 for β_{PSII} and 0.69 for α_{PSII} (Supplemental Fig. S7, B and D).

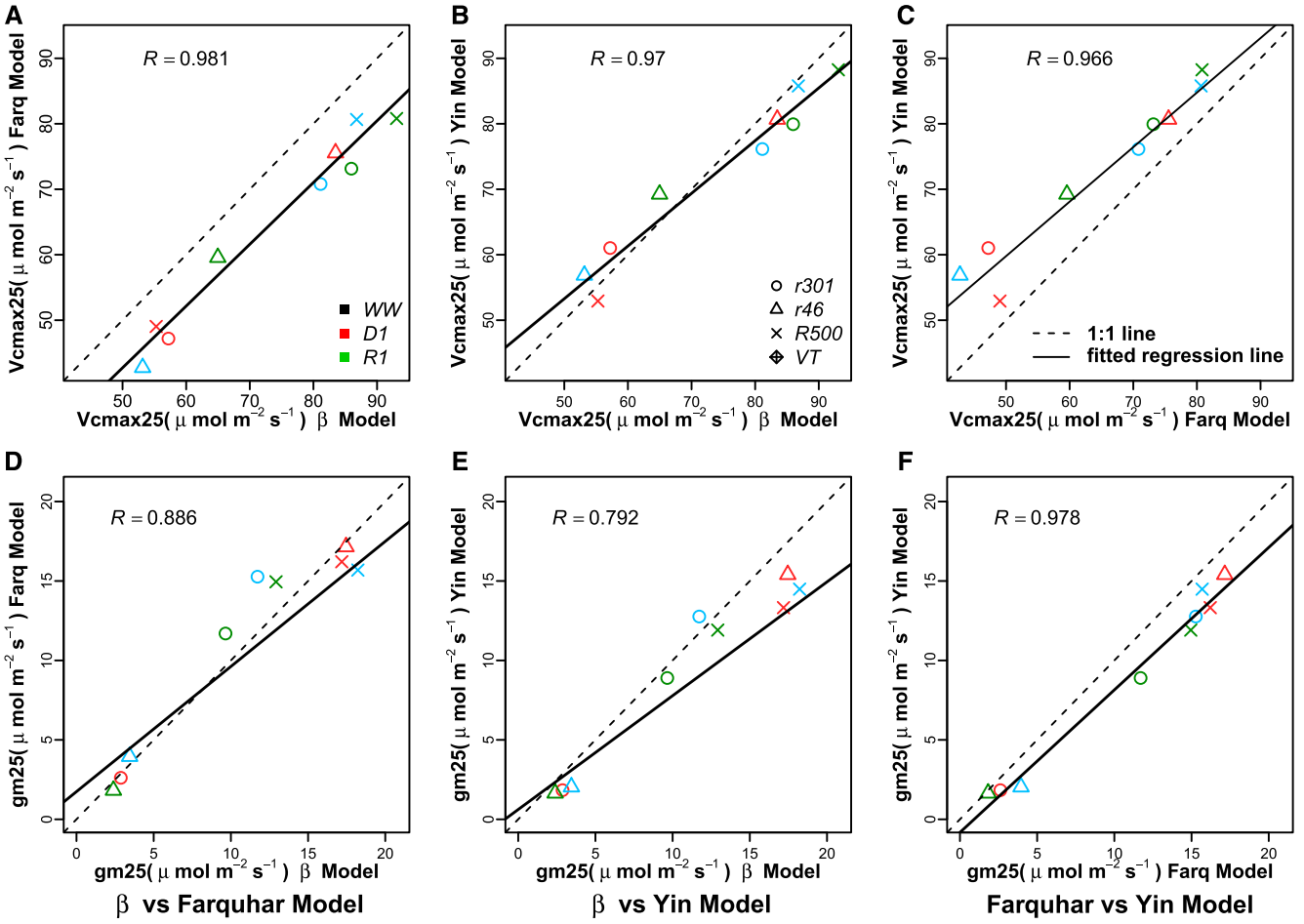

Figure 4. Comparison of posterior median estimates of parameters common to the FvCB, Yin, and β_{PSII} photosynthesis models. A to C, Comparison of V_{cmax} estimates between β_{PSII} and FvCB, β_{PSII} and Yin, and FvCB and Yin with R for each relationship. D to F, Comparison of g_m estimates between β_{PSII} and FvCB, β_{PSII} and Yin, and FvCB and Yin with R for each relationship. Genotypes and water regimes are as defined in Figure 2.

DISCUSSION

Here, we tested how applying alternative descriptions of quantum yield (ϕ_{CO2}, ϕ_{PSII}, and β_{PSII}) in photosynthesis models (Fig. 1) can improve the mechanistic realism of electron transport processes and their potential changes under drought. Our β_{PSII} photosynthesis model utilized the full ϕ_{PSII} versus Q response, accounting for possible photoprotective mechanisms (i.e. NPQ, changes in absorbance, etc.). All these mechanisms decrease photosynthetic ETR and play crucial roles in the A_n magnitude under stress, and we have to consider and quantify them to mechanistically improve simulated responses to drought and other environmental changes.

β_{PSII} Dynamics

Our main goal was to explore the use of chlorophyll *a* fluorescence parameters derived from rapid light curves, collected with a dynamic high-throughput tool, to develop a photosynthesis model for estimating photosynthetic ETR. The major design improvement of the MultispeQ is the quick capture of fluorescence parameters precisely during steady-state illumination (Kuhlgert et al., 2016), and we tested the relationship between rapid fluorescence data from the MultispeQ and the LiCOR 6400-40 fluorimeter (Fig. 6). Single-measurement comparisons grouped by genotype show linear relationships across different light levels and water treatment, with $R^2 > 0.9$ despite the variations in time of day, duration of the actinic light, etc., between the low- and high-throughput measurements due to the fact that the LiCOR instrument is primarily utilized to take simultaneous measurements of gas exchange. Our results build on previous work by Meacham et al. (2017), who posed the question about the use of rapid fluorescence analysis for photosynthesis modeling. However, we experimented beyond their results, using the high-throughput MultispeQ instead of a monitoring PAM device from Walz, thus avoiding the use of aluminum foil to cover the leaves during the measurements and the possible increases in temperature with consequent

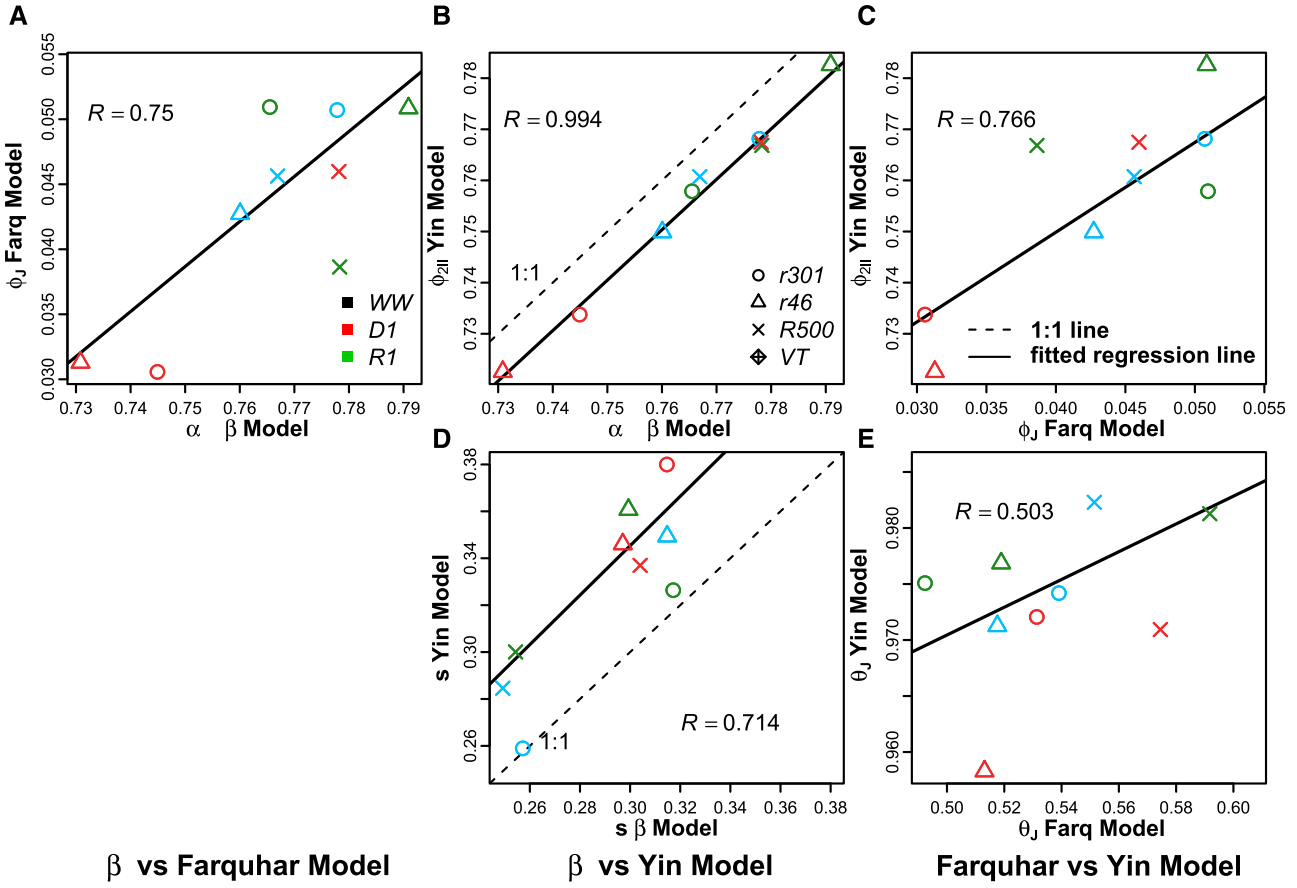

Figure 5. Comparison of posterior median estimates of parameters in the FvCB, Yin, and β_{PSII} models. A to C, Comparison of quantum yield terms for each model: α_{PSII} (mol photon mol^{-1} e^{-}) of the β_{PSII} model with ϕ_{CO2} (mol CO_2 mol^{-1} e^{-}) of the FvCB model (A), α_{PSII} with ϕ_{PSII_II} (mol photon mol^{-1} e^{-}) of the Yin model (B), and ϕ_J with ϕ_{PSII_II} (C) with correlation coefficient (R) for each. D and E, Comparison of the s parameter between the Yin model and the β_{PSII} model (D) and comparison of θ_J between the Yin model and the FvCB model (E). Genotypes and water regimes are as defined in Figure 2.

changes in water vapor exchange (Giorio, 2011; Bücher et al., 2018). Rapid light curves are complex to interpret due to the presence of several components in the photosynthetic apparatus characterized by different time constants (i.e. the time to reach ~63% of the full response) involved (Pearcy, 1990; Way and Pearcy, 2012). We acknowledge that light harvesting and energy transfer respond nearly instantaneously to changes in the light environment, whereas adjustments in the carbon cycle metabolites can take up to several seconds (Powles, 1984; Geiger and Servaites, 1994). However, the use of a fast analysis is necessary to capture the true light conditions of plants in the field, where they rarely photosynthesize at full capacity (Ort and Melis, 2011). Fast changes in incoming radiation, such as that used during the collection of rapid light curves, can be thought to have similar consequences as for leaves exposed to sunflecks. After an initial uncoupling of the electron transport from CO_2 fixation, the metabolite pool has been shown to refill within a few seconds in healthy leaves (Parry et al., 2008; McClain and Sharkey, 2019). The fluorescence calculated parameters have already been shown to have a very dynamic behavior (Porcar-Castell et al., 2012), which leaves room to accommodate for stress-related mechanisms.

The exponential decline of ϕ_{PSII} versus Q (Eq. 1) takes into account changes occurring at PSII antenna reaction center complexes and is extremely relevant under stress conditions. These changes are not included in current photosynthesis models (Fig. 1). Identifying the parameter β_{PSII}, meaning the rate of decline of ϕ_{PSII} at Q increase, and its dynamics at the onset of water stress is highly valuable to mechanistically elucidate processes of photoprotection and increased photorespiration, which are relevant for the overall reduction of assimilation under stress (Ort and Baker, 2002; Souza et al., 2004). The ϕ_{PSII} and Q relationship has been previously used to assess photosynthetic responses using the ETR maximum, showing declines under water stress (Rascher et al., 2004; Li et al., 2008; Batra et al., 2014).

Our results depict a more complete picture of the changes in ϕ_{PSII} versus Q under drought, and the parameter β_{PSII} seems to be better suited to explain a range of stress responses (Figs. 2 and 3). The observed

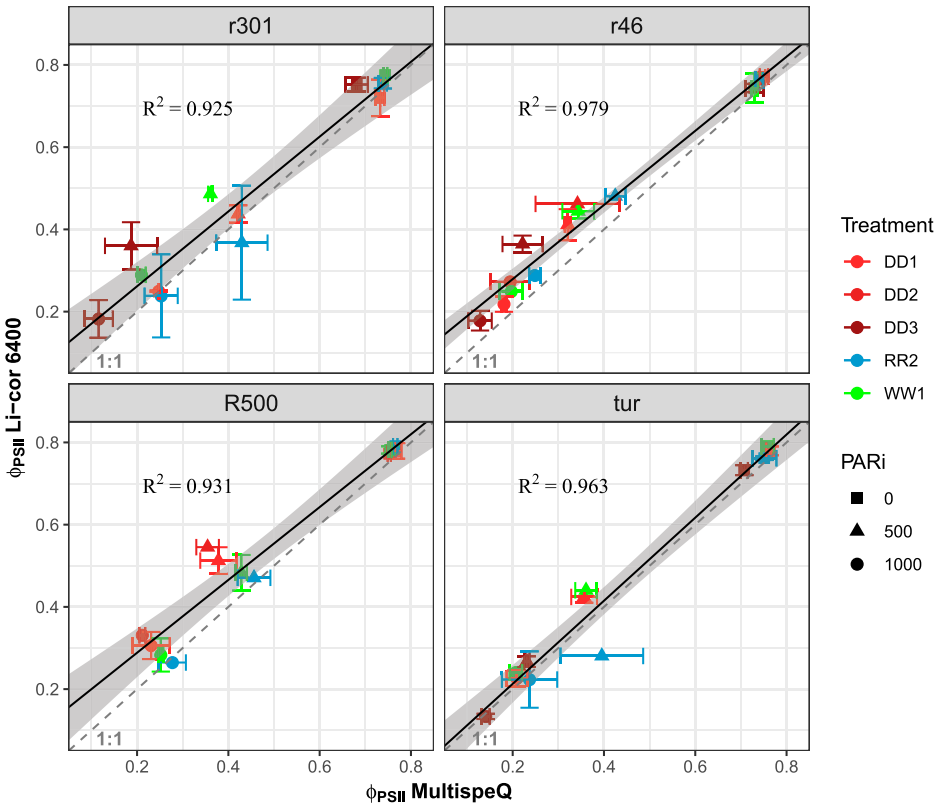

Figure 6. PSII efficiency instrumentation correlation. Comparison of ϕ_{PSII} across two instruments, LiCOR 6400 and MultispeQ, and three light intensities (0, 500, and 1,000 μmol photons m^{-2} s^{-1} photosynthetically active radiation [PARi]) for the four *B. rapa* genotypes *r301* (A), *r46* (B), *R500* (C), and *VT* (D). Each set of observations occurred over a range of water regimes from well-watered (W1) to increasing drought (D1–D3) and rewatering (R2). Points are means of replicates, and error bars represent SD (total *n* LiCOR 6400 = 162, average *n* per replicate = 2.7; total *n* MultispeQ = 213, average *n* per replicate = 3.6).

declines in β_{PSII}, here observed under drought, may in fact be the result of more or less regulated processes, such as NPQ (Table 3), chloroplast light avoidance, and nonregulated energy dissipation (Müller et al., 2001; Kasahara et al., 2002; Takahashi and Badger, 2011). Furthermore, the modest recovery after a 6-h period in both β_{PSII} and α_{PSII} suggests that these parameters account for more than just fast-regulated photoprotective mechanisms (Dall'Osto et al., 2005; Lambrev et al., 2012). Nearly full recovery by 30 h after the start of rewatering may be due to slow-relaxing and/or unregulated processes, along with protein turnover and repair processes that require a longer time to return to prestress conditions (Nishiyama et al., 2006; Brooks et al., 2013; Malnoë, 2018). Indeed, both slow and rapid light curves are able to trigger slow-relaxing NPQ mechanisms (qI), with qI having lifetime changes similar to those observed during qE (rapid relaxing mechanisms; Müller et al., 2001; Lazár, 2015; Ruban, 2016).

Both β_{PSII} and α_{PSII} depicted genotypic variation relative to drought severity, with *r301* showing greatest declines (i.e. transgressive segregation with respect to the RIL parents), followed by *R500* and *VT*, which accumulate the highest amount of aboveground biomass (Fig. 3, B and F). Future work should consider how the slope of variation in the ϕ_{PSII} versus Q response relates to previous findings of root-shoot allocation differences occurring under drought (Edwards et al., 2016) as well as explore how variance in β_{PSII} may influence reactive oxygen species production and, when more pronounced declines occur, cellular damage (Reddy et al., 2004).

Implementing Photosynthesis Modeling

Using direct observations of ϕ_{PSII} versus Q data as parameters in a leaf photosynthesis model provided a means of quantifying the impacts of PSII photoprotective mechanisms on ETR. Although these protective processes are critical to final net photosynthesis, they are abstracted out of all FvCB-based modeling efforts (Horton et al., 1994; Allen and Pfannschmidt, 2000; Laisk et al., 2002); therefore, current parameterization approaches may be biased by tuning parameters without mechanistic insight. Our β_{PSII} approach extends the development of FvCB-based models using both A/C_i and light response curves in analysis (Holland, 2007; Patrick et al., 2009) to integrate both gas-exchange and fast chlorophyll *a* fluorescence observations into models (Laisk and Loreto, 1996; Laisk et al., 2002; Yin et al., 2006, 2009). The β_{PSII} photosynthesis model maintains the use of commonly employed parameters, such as V_{cmax}, R_d, and g_m, while shifting away from others, such as J_{max} and θ_J, that do not fully incorporate stress impacts on ETR, for describing ETR and associated processes. Estimates of the common parameters including V_{cmax} show strong similarity across the three considered photosynthetic models (Fig. 4). The correlations between the β_{PSII} with V_{cmax}

and J_{max} estimates of the FvCB and Yin models is promising for model parameterization. The throughput of ϕ_{PSII} versus Q measurements will also increase the number of genotypes used in models and thus better incorporate mechanistically rigorous, genotype-level informed parameters for crop simulation (Boote et al., 2001; Bertin et al., 2010; Archontoulis et al., 2012; Pleban et al., 2018).

The lumped s parameter has a valuable role in accommodating a number of mechanisms affecting the final ETR and showed declines after 13 d of drought (Supplemental Fig. S3). Our photosynthesis model is able to assess the extent of the mechanisms slowing down ETR as a whole. However, the same MultispeQ collects fluorescence values at each recorded pulse. All components of NPQ (qE, qT, and qI) could then be calculated from values of F_m' and F_m over time, allowing for a detailed energy partitioning analysis. These results could benefit the model and separate physiological (feedback mechanisms) and damage consequences of the stress. Future work, including the use of knockout mutants, such as those for genes involved in NPQ mechanisms, will be needed to disentangle the three factors lumped in s (f_{alt}, α_{leaf}, and ρ_2). Changes in relative chlorophyll and SPAD at 540 nm affect the overall leaf absorbance (α_{leaf}) and are partially responsible for changes in s (Table 3). Future work evaluating the light-harvesting properties of photosynthetic pigment molecules will help clarify the importance of this component on the lumped s. Isolating changes in α_{leaf} might also use statistical methods to identify dominant shifts in absorption from spectrophotometric data (Baker et al., 2018). It appears likely that the other two factors, f_{alt} and ρ_2, changed during drought progression, based on the decline in LEF relative to increases in ECS_t (Table 3). We speculate that the altered relationship between LEF and ECS_t may relate to energetic spillover and changes in cross-membrane ΔH^+ triggering unbalanced activity in the PSII-PSI duo, ultimately leading to an increased cyclic electron flow around PSI (Livingston et al., 2010; Strand et al., 2015). Future data-model integration could consider saturation pulse estimation of PSI yield parameters to quantify the specific contribution of f_{alt} and ρ_2 (Klughammer and Schreiber, 1994). Integration with ECS_t data could also assist in understanding the potential for change in how transthylakoidal ΔH^+ might be coordinated by the use of cyclic and other nonlinear electron transport pathways (Kramer et al., 2004b).

Our framework offers opportunities to better evaluate stress limitations on quantum yield and ETR. The coupling of s and β_{PSII} as described here is critical for future efforts to model individual photoprotective, photoinhibitory, and photodamaging mechanisms, which are encompassed in these two parameters, albeit in a lumped way. Further implementation of current instrumentation and further modeling approaches may allow for itemizing specific physiological or genetic mechanisms underlining s and β_{PSII} responses to drought (Noctor et al., 2002; Miller et al., 2010; Guadagno et al., 2017).

β_{PSII} Photosynthesis Model Limitations

Our approach needs additional tests under natural and/or higher intensity light conditions to investigate details of photoprotective mechanisms and their behavior under extreme environmental conditions. For instance, the ratio of carotenoids in the PSII antenna complex responsible for NPQ can vary with growing conditions (Kato et al., 2003). Furthermore, photodamage has been shown to be more severe in the UV range and at 500 to 600 nm, and the ratio of photodamage to repair is higher as light intensity increases (Nogués and Baker, 2000; Murata et al., 2007; Zavafer et al., 2015). Also, dynamic fluctuations in light, such as those in natural settings, can have relevant effects on photosynthetic rate (Vialet-Chabrand et al., 2016, 2017), which we expect are more severe under drought, with subsequent recovery processes possibly delayed (Fig. 3). The repair of PSII damage can also be compromised by temperature stress (Murata et al., 2007). Consequently, how β_{PSII}, α_{PSII}, and s respond to field conditions, drought, and other stresses should be further investigated.

The difficult estimation of g_m may also affect further implementation of our framework, and alternative methods of g_m assessment should be considered. The g_m estimation in all three photosynthesis models used the combined fluorometry/gas-exchange approach (Harley et al., 1992; Pons et al., 2009; Archontoulis et al., 2012). Two of the three models (Yin and β_{PSII}) included the s parameter to consider alternative electron pathways influencing the g_m estimation (Fig. 4, D–F). State-of-the-art photosynthesis models include a dynamic g_m responding to variations in both internal leaf status and external environments (Tazoe et al., 2009; Moualeu-Ngangue et al., 2017). Coupling online isotope discrimination data to the linear and total electron flow, gathered from gas-exchange and fluorometry observations, may help resolve concerns related to g_m estimation and allow for the integration of a dynamic g_m model into the β_{PSII} method (Pons et al., 2009; Tazoe et al., 2009; Gu and Sun, 2014; Moualeu-Ngangue et al., 2017; Flexas et al., 2018).

Predictive understanding of both photoprotective and g_m mechanisms is still in its infancy; the alternative approach we have successfully tested provides a crucial transfer of high-throughput empirical measurements and analyses to mechanistic simulations that are likely to improve predictive understanding of drought and other stress responses across a range of plant species and genotypes. Our β_{PSII} model will further the improvements of current whole-plant crop modeling by the incorporation of first-principles mechanisms (Hammer et al., 2006; Chenu et al., 2009; Wang et al., 2019) through the incorporation of more genetic and omic information into the parameters of biophysical-based models.

MATERIALS AND METHODS

Plant Material

Four genotypes of *Brassica rapa* were utilized for our analysis: two crop accessions, *R500* (oilseed crop, *B. rapa* ssp. *trilocularis* ['Yellow Sarson']) and *VT*

(VT-089, D'Auvergne Hative); and two RILs (*r46* and *r301*). The RILs are part of a population developed from a cross between the *R500* × *Imb211* genotypes. The *R500* genotype is an oilseed cultivar planted in India for approximately 3,000 years (Prakash and Hinata, 1980) with large allocation to seed production (Baker et al., 2015). The *Imb211* genotype is a rapid-cycling line derived from the Wisconsin Fast Plant (Williams and Hill, 1986). The extremely divergent selection history suggests that genetic variation segregating in the RILs may resemble that segregating in crop × wild hybrids found commonly in nature (Adler et al., 1993). The RIL population has been previously described, and the two RILs of interest were chosen based on their transgressively segregating drought stress phenotypes identified in earlier research (Iniguez-Luy et al., 2009; Edwards et al., 2011, 2012; Pleban et al., 2018). Seeds of *R500*, *r46*, and *r301* were obtained from a single-seed collection bulked at the University of Wyoming in 2011. *VT* was obtained from the Wageningen University and Research Center for Genetic Resources (CGN#10995).

Growth Conditions

Seeds were germinated and grown in pots (500 mL) filled with a soil mixture (Miracle-Gro Moisture Control Potting Mix [20%, v/v] and Profile Porous Ceramic Greens Grade [80%, v/v]) with the addition of 2 mL of Osmocote 18-6-12 fertilizer (Scotts). Experiments occurred during July and August 2017 at the University at Wyoming in three growth chambers (PGC-9/2; Percival Scientific). Growth chamber conditions were set at a 14-h photoperiod of approximately 250 to 300 μmol photons $m^{-2}\,s^{-1}$ Q, with a 25°C to 30°C/18°C to 22°C day/night cycle, and relative humidity maintained at 45% to 65%. Soil moisture content was monitored daily for all treatment groups (ECH_2O/EC5 probe; Decagon). Plants were randomized in three growth chamber compartments with blocks of each treatment, with a randomized mix of four genotypes present in each compartment.

For 4 weeks, all plants were regularly watered to maintain VWC at 0.3 ± 5. At 28 d after sowing, watering was withheld from treatment plants in the droughted and rewatered cohorts (Supplemental Fig. S1). On experimental day 0, drought was applied via complete water withholding for the droughted cohort. Droughted plants were assigned to three different groups and replicate plants observed on experimental days 4 to 7 (treatment group D1), 9 to 12 (treatment group D2), and 15 (treatment group D3). On experimental day 9, water was reapplied to a subset of droughted plants (R1), and they were observed on experimental days 9 to 12. On experimental day 15, a second subset of droughted plants (R2) was rewatered and observed 6 h after rewatering. Finally, on day 16, the last subset of droughted plants was rewatered and assessed at 30 h after rewatering (R3). Soil moisture observations in this study were comparable to those from Guadagno et al. (2017), where the mean VWC was 0.06 ± 0.01 after 14 d of drought; here, the mean VWC after 13 d of drought was 0.05 ± 0.03.

Plant Physiological Observations

Physiological data collection followed the temporal frequency in Supplemental Figure S1. For evaluation of photosynthesis traits throughout the treatment period, A/C_i curves and photosynthetic light response curves were taken (LiCOR 6400XT; LI-COR Biosciences) following established methods (Long and Bernacchi, 2003). Both response curves were measured between 10 AM and 4 PM on fully expanded leaves (between fifth and eighth leaves) with cuvette settings at a flow rate of 300 μmol s^{-1}, relative humidity maintained at 50% ± 8%, and temperature maintained at 20°C. A/C_i curves set sample chamber CO_2 concentrations to 50, 100, 200, 300, 400, 500, 600, 800, 1,000, 1,250, 1,500, and 2,000 μmol CO_2 mol^{-1} air. A/C_i curves were taken on WW, D1, and R1 plants. Light response curves were measured across 10 light conditions (Q = 2,000, 1,500, 1,000, 500, 250, 125, 60, 30, 15, and 0 μmol photons $m^{-2}\,s^{-1}$). Light response curves were taken on WW, D1, and R1 as well as D2 and D3 plants. For both response curves, PAM fluorescence was measured immediately after gas exchange using a leaf chamber fluorimeter (LiCOR 6400-40; LI-COR Biosciences). With actinic light maintained at setting of curve protocol (λ = 470 nm, 10% blue to obtain values of F_s), a short saturating pulse (0.8 s; ~8,000 μmol photons $m^{-2}\,s^{-1}$) was applied to measure F_m' with a short far-red pulse to record the F_o' value at the end of induction (Baker, 2008). These were used to determine the operating efficiency of PSII photochemistry, $(F_m' - F_s)/F_m' = \phi_{PSII}$, for light-acclimated conditions (Genty et al., 1989). Fluorescence measurements were taken in conjunction with all changes in C_i or Q for each A/C_i and light response curve.

Further chlorophyll fluorescence observations used a rapid PAM light response protocol developed for the MultispeQ spectrophotometer (PhotosynQ). The protocol is available on the PhotosynQ platform under project title: *B. rapa* drought and recovery Chl Fl evaluation (https://photosynq.org/projects/b-rapa-drought-and-recovery-chl-fl-evaluation). In a single 5-min clamping with a fully expanded leaf (between fifth and eighth leaves), actinic light (655 nm [Lumileds; LXZ1-PA01]) was incremented at 10 light intensities (1,000, 800, 600, 500, 400, 300, 200, 100, 50, and 0 μmol photons $m^{-2}\,s^{-1}$) for 30 s before a PAM fluorometry sequence was initiated following established methods (Rascher et al., 2000; Datko et al., 2008). After each light acclimation period, the PAM sequences used the classic multiphase flash technique with four rectangular saturation flashes of 4,500, 4,050, 3,600, and 3,150. A linear regression of each maximum fluorescence ramp versus $1/Q$ was made to determine expected F_m', used for calculating fluorescence parameters. Recently, the original derivation of NPQ was extended to NPQ_t, allowing for high-throughput (under 1 min each) yet mechanistically relevant measurements (Tietz et al., 2017). Therefore, this protocol assessed ϕ_{PSII}, the fraction of Q dissipated safely as heat (ϕ_{NPQt}), and the fraction of Q quenched via unregulated excitation dissipation (ϕ_{NO}) at each light intensity. ϕ_{NPQt} assumes a constant theoretical maximum dark-adapted fluorescence yield, and ϕ_{NO} represents the fraction of light use remaining after accounting for ϕ_{NPQt} and ϕ_{PSII} [$\phi_{NO} = 1 - (\phi_{NPQt} + \phi_{PSII})$; Tietz et al., 2017]. From these response curves, LEF was calculated for each Q following $LEF = \phi_{PSII}\,Q\,\alpha_{leaf}\,\rho_2$, where α_{leaf} is assumed to be 0.85 and ρ_2 is assumed to be 0.5. Rapid PAM light response curves were taken on plants from each watering cohort (Supplemental Fig. S1).

Total *ECSt* measurements were obtained at two Q intensities (300 and 1,000 μmol photons $m^{-2}\,s^{-1}$ at 650 nm) using the MutlispeQ (Kuhlgert et al., 2016). *ECSt* monitors the proton flow into the thylakoid lumen by evaluating shifts in the absorbance of cross-membrane carotenoid pigments (Fig. 1, blue H^+ arrows). The carotenoid absorbance spectrum is dependent on the changing electrical gradient produced by proton flow across the thylakoid membrane (Sacksteder et al., 2000). The protocol for these *ECSt* observations is available on the PhotosynQ platform (https://photosynq.org/projects/b-rapa-drought-and-recovery-ecs-evaluation). *ECSt* observations were taken on plants of all watering cohorts (Supplemental Fig. S1). Observations of relative chlorophyll content were also measured with a hand-held MultispeQ spectrophotometer on plants of all watering cohorts (Supplemental Fig. S1).

Exponential Decline of ϕ_{PSII} Versus Q

Light response data, ϕ_{PSII}, from both the LiCOR fluorimeter and the MultispeQ rapid fluorescence protocol were used to model the decline in ϕ_{PSII} under increasing Q. A hierarchical Bayesian framework generated genotype × treatment posterior trait distributions of exponential decline parameters. A three-parameter exponential decline function was used following Equation 1:

$$\phi_{PSII} = (\alpha_{PSII} - \kappa_{PSII})e^{Q\beta_{PSII}} + \kappa_{PSII}$$

where α_{PSII} (y intercept) represents the maximum light-adapted ϕ_{PSII}, β_{PSII} represents the exponential decline rate in ϕ_{PSII} under increasing Q, and κ_{PSII} represents a non-zero minimum of ϕ_{PSII} as Q approaches ∞. Equation 1 was modeled using rjags (Plummer, 2014), with samples from the posterior parameter distributions generated from a Gibbs sampling method (Plummer, 2003). Model parameters (α_{PSII}, β_{PSII}, and κ_{PSII}) were estimated using a three-level hierarchical structure with global, genotype × treatment, and individual plant levels. Priors for the means of the exponential decline parameters followed wide informed normal distributions broadly informed with wide variances. Priors for the precision terms used weakly informed normal distributions (Gelman, 2006). The credible interval divergence at 95% HDI was used to evaluate posterior parameter differences for each treatment time. This comparison metric used in Bayesian analysis allows the identification of definitive portions of the posterior distributions characterized by higher probability density than the regions outside those intervals (Kruschke, 2014, 2018; Kruschke and Liddell, 2018), with more rigorous results and higher predictive power.

Photosynthesis Modeling

Utilizing Bayesian statistics, all photosynthesis models describe how quantum yield and underpinning mechanisms are related to CO_2 assimilation

under changing light conditions and water availability. The three model formulations are similar to those found in photosynthesis process models while hierarchically incorporating uncertainty and providing probabilistic quantification of parameters. Tables 1 and 2 outline the three modeling approaches used to test the utility of ϕ_{PSII} light response data for characterizing ETR and light-limited A_n. All three approaches estimate A_n following Equation 2.1 with the estimation of the critical C_i (C_{crit}), where A_c shifts to A_J, following methods detailed below. All three approaches estimate A_c using Equations 2.2 and 2.3 (Table 2). The approaches vary in the derivation of photosynthetic ETR. The first approach followed the FvCB model, estimating ETR using information from leaf gas exchange (Eq. 2.5; Farquhar et al., 1980; Farquhar and Wong, 1984; Fig. 1A). This FvCB derivation of ETR for A_J (J_m) requires estimation of three parameters: J_{max}, the maximum rate of electron transport; ϕ_{CO2}, the quantum yield on a CO_2-to-photon basis; and θ_J, the convexity factor for the response of ETR to Q. Two other parameters are fixed a priori in FvCB: an equal fractionation of light between PSI and PSII ($\rho_2 = 0.5$), and leaf absorbance (α_{leaf}) is set at 0.85. The second approach, described by Yin et al. (2009), used a combined gas-exchange and fluorescence approach for modeling ETR (J_f; Fig. 1B). The Yin model used ϕ_{PSII} data to parameterize PSII efficiency under limiting light (ϕ_{PSII_ll}) as well as the lumped parameter, s, which lumps α_{leaf} differences, differences in ρ_2, as well as utilization of alternate electron paths, f_{alt}, along the Z-scheme (Eq. 2.6). Low-light ($0 < Q < 200$ μmol photon m^{-2} s^{-1}) response data (A_n, Q, and ϕ_{PSII}) were subset to estimate R_d, s, and ϕ_{PSII_ll} in the Yin model. R_d is estimated as the y intercept of linear regression of A_n against $\frac{Q\phi_{PSII}}{4}$. The slope of this regression is used to estimate s. The quantum yield parameter for the Yin model, ϕ_{PSII_ll}, was estimated as the y intercept of a linear regression of A_n against ϕ_{PSII} under low Q. Finally, for the third approach, the β_{PSII} photosynthesis model derivation ETR (J_l), the full light response ϕ_{PSII} data set was passed in the β_{PSII} model for the estimation of α_{PSII}, β_{PSII}, or κ_{PSII} needed to describe ETR (J_l; Fig. 1C). Following Equation 1, the α_{PSII}, β_{PSII}, and κ_{PSII} estimates were used to predict ϕ_{PSII} at each Q, next J_l was solved following Equation 2.7. β_{PSII} implementation used the same R_d and s estimation as Yin.

All models used a temperature response following an Arrhenius function for K_c, K_o, V_{cmax}, J_{max}, g_m, R_d, and Γ^*. Each parameter was normalized with respect to 25°C following:

$$X = X_{25} \exp\left[\frac{E_x\left(T_{leaf} - 25\right)}{298\ R\left(T_{leaf} + 273\right)}\right] \quad (3)$$

where T_{leaf} is leaf temperature (°C), X_{25} is the parameter normalized with respect to 25°C, E_X is the activation energy of each parameter, and R is the universal gas constant (8.314 J K^{-1} mol^{-1}). Other temperature response functions were considered, but given the limited variability in T_{leaf} (mean = 20 ± 0.2), a simple one-parameter equation was selected for analysis.

C_{crit}, the C_i at which A_n transitions from A_c to A_J, was fixed at 285 ppm in all models based on an analysis of $F_v'F_m'$ under increasing C_i. $F_v'F_m'$ increases when $C_i < C_{crit}$ and remains constant when $C_i > C_{crit}$ (Sharkey et al., 2007; Gu et al., 2010; Moualeu-Ngangue et al., 2017). A Bayesian model was employed using a single change point method (Dose and Menzel, 2004) to estimate individual and population-level C_{crit}. Results of the change point model found that the posterior population level estimate had a mean of 287.3 with a 95% HDI of 265.1 to 318.7 ppm (Supplemental Fig. S8).

All C_i, A_n, Q, and T_{leaf} data from A/C_i and light response curves were used to estimate A_n traits, an approached used previously (Patrick et al., 2009; Archontoulis et al., 2012), with ϕ_{PSII} data supplied to the Yin and β_{PSII} models as described above. Parameter priors for FvCB and shared parameters among the three models were selected based on a recent implementation (Pleban et al., 2018). The code for all three photosynthesis models as well as the simple β_{PSII} decline model are available at https://github.com/jrpleban/.

Supplemental Data

The following supplemental materials are available.

Supplemental Figure S1. Experimental design and observation schedule.

Supplemental Figure S2. Volumetric soil water content dynamics.

Supplemental Figure S3. Changes in lumped s parameter estimates.

Supplemental Figure S4. Onset of the NPQt parameter.

Supplemental Figure S5. Simulated A_n versus observed A_n for three photosynthesis models.

Supplemental Figure S6. Correlations of β_{PSII} with classic photosynthetic model parameters.

Supplemental Figure S7. Decline rates of PSII efficiency under changing light conditions.

Supplemental Figure S8. Identification of the transition point between A_c and A_J (C_{crit}).

ACKNOWLEDGMENTS

We thank Christopher Nieters, Sara Lemli, and Shea Ruggier for assistance in data collection. We thank Xiaonan Tai, Dan Potts, and Diane R. Wang for feedback during article preparation.

Received February 6, 2020; accepted February 18, 2020; published March 9, 2020.

LITERATURE CITED

Adler LS, Wikler K, Wyndham FS, Linder CR, Schmitt J (1993) Potential for persistence of genes escaped from canola: Germination cues in crop, wild, and crop-wild hybrid *Brassica rapa*. Funct Ecol **7:** 736–745

Allen JF, Pfannschmidt T (2000) Balancing the two photosystems: Photosynthetic electron transfer governs transcription of reaction centre genes in chloroplasts. Philos Trans R Soc Lond B Biol Sci **355:** 1351–1359

Archontoulis SV, Yin X, Vos J, Danalatos NG, Struik PC (2012) Leaf photosynthesis and respiration of three bioenergy crops in relation to temperature and leaf nitrogen: How conserved are biochemical model parameters among crop species? J Exp Bot **63:** 895–911

Asada K (2006) Production and scavenging of reactive oxygen species in chloroplasts and their functions. Plant Physiol **141:** 391–396

Baker NR (2008) Chlorophyll fluorescence: A probe of photosynthesis in vivo. Annu Rev Plant Biol **59:** 89–113

Baker RL, Leong WF, Brock MT, Markelz RJ, Covington MF, Devisetty UK, Edwards CE, Maloof J, Welch S, Weinig C (2015) Modeling development and quantitative trait mapping reveal independent genetic modules for leaf size and shape. New Phytol **208:** 257–268

Baker RL, Leong WF, Welch S, Weinig C (2018) Mapping and predicting non-linear *Brassica rapa* growth phenotypes based on bayesian and frequentist complex trait estimation. G3 (Bethesda) **8:** 1247–1258

Batra NG, Sharma V, Kumari N (2014) Drought-induced changes in chlorophyll fluorescence, photosynthetic pigments, and thylakoid membrane proteins of *Vigna radiata*. J Plant Interact **9:** 712–721

Bellasio C, Beerling DJ, Griffiths H (2016) An Excel tool for deriving key photosynthetic parameters from combined gas exchange and chlorophyll fluorescence: Theory and practice. Plant Cell Environ **39:** 1180–1197

Bertin N, Martre P, Génard M, Quilot B, Salon C (2010) Under what circumstances can process-based simulation models link genotype to phenotype for complex traits? Case-study of fruit and grain quality traits. J Exp Bot **61:** 955–967

Boote KJ, Kropff MJ, Bindraban PS (2001) Physiology and modelling of traits in crop plants: Implications for genetic improvement. Agric Syst **70:** 395–420

Bota J, Medrano H, Flexas J (2004) Is photosynthesis limited by decreased Rubisco activity and RuBP content under progressive water stress? New Phytol **162:** 671–681

Brooks MD, Sylak-Glassman EJ, Fleming GR, Niyogi KK (2013) A thioredoxin-like/β-propeller protein maintains the efficiency of light harvesting in Arabidopsis. Proc Natl Acad Sci USA **110:** E2733–E2740

Bücher SF, Bernhardt–Römermann M, Römermann C (2018) Chlorophyll fluorescence and gas exchange measurements in field research: An ecological case study. Photosynthetica 1161–1170

Chenu K, Chapman SC, Tardieu F, McLean G, Welcker C, Hammer GL (2009) Simulating the yield impacts of organ-level quantitative trait loci associated with drought response in maize: a "gene-to-phenotype" modeling approach. Genetics **183:** 1507–1523

Cruz JA, Savage LJ, Zegarac R, Hall CC, Satoh-Cruz M, Davis GA, Kovac WK, Chen J, Kramer DM (2016) Dynamic environmental photosynthetic imaging reveals emergent phenotypes. Cell Syst **2:** 365–377

Dall'Osto L, Caffarri S, Bassi R (2005) A mechanism of nonphotochemical energy dissipation, independent from PsbS, revealed by a conformational change in the antenna protein CP26. Plant Cell **17:** 1217–1232

Datko M, Zivcak M, Brestic M (2008) Proteomic analysis of barley (*Hordeum vulgare* L.) leaves as affected by high temperature treatment. *In* JF Allen, E Gantt, JH Golbek, and B Osmond, eds, Photosynthesis: Energy from the Sun. Springer, Dordrecht, Germany, pp 1523–1527

de Witt CT (1966) Agricultural Research Report: Photosynthesis of Leaf Canopies. Centre for Agricultural Publications and Documentation, Wageningen, The Netherlands

Dose V, Menzel A (2004) Bayesian analysis of climate change impacts in phenology. Glob Change Biol **10:** 259–272

Drake JE, Power SA, Duursma RA, Medlyn BE, Aspinwall MJ, Choat B, Creek D, Eamus D, Maier C, Pfautsch S, et al (2017) Stomatal and non-stomatal limitations of photosynthesis for four tree species under drought: A comparison of model formulations. Agric For Meteorol **247:** 454–466

Edwards CE, Ewers BE, McClung CR, Lou P, Weinig C (2012) Quantitative variation in water-use efficiency across water regimes and its relationship with circadian, vegetative, reproductive, and leaf gas-exchange traits. Mol Plant **5:** 653–668

Edwards CE, Ewers BE, Weinig C (2016) Genotypic variation in biomass allocation in response to field drought has a greater affect on yield than gas exchange or phenology. BMC Plant Biol **16:** 185

Edwards CE, Ewers BE, Williams DG, Xie Q, Lou P, Xu X, McClung CR, Weinig C (2011) The genetic architecture of ecophysiological and circadian traits in *Brassica rapa*. Genetics **189:** 375–390

Farquhar GD, von Caemmerer S, Berry JA (1980) A biochemical model of photosynthetic CO_2 assimilation in leaves of C 3 species. Planta **149:** 78–90

Farquhar GD, Wong SC (1984) An empirical model of stomatal conductance. Aust J Plant Physiol **11:** 191–210

Filek M, Łabanowska M, Kościelniak J, Biesaga-Kościelniak J, Kurdziel M, Szarejko I, Hartikainen H (2015) Characterization of barley leaf tolerance to drought stress by chlorophyll fluorescence and electron paramagnetic resonance studies. J Agron Crop Sci **201:** 228–240

Fini A, Guidi L, Ferrini F, Brunetti C, Di Ferdinando M, Biricolti S, Pollastri S, Calamai L, Tattini M (2012) Drought stress has contrasting effects on antioxidant enzymes activity and phenylpropanoid biosynthesis in *Fraxinus ornus* leaves: An excess light stress affair? J Plant Physiol **169:** 929–939

Flexas J, Bota J, Escalona JM, Sampol B, Medrano H (2002) Effects of drought on photosynthesis in grapevines under field conditions: An evaluation of stomatal and mesophyll limitations. Funct Plant Biol **29:** 461–471

Flexas J, Carriquí M, Nadal M (2018) Gas exchange and hydraulics during drought in crops: Who drives whom? J Exp Bot **69:** 3791–3795

Flexas J, Medrano H (2002) Drought-inhibition of photosynthesis in C3 plants: Stomatal and non-stomatal limitations revisited. Ann Bot **89:** 183–189

Flood PJ, Kruijer W, Schnabel SK, van der Schoor R, Jalink H, Snel JF, Harbinson J, Aarts MG (2016) Phenomics for photosynthesis, growth and reflectance in Arabidopsis thaliana reveals circadian and long-term fluctuations in heritability. Plant Methods **12:** 14

Franks SJ (2011) Plasticity and evolution in drought avoidance and escape in the annual plant *Brassica rapa*. New Phytol **190:** 249–257

Geiger DR, Servaites JC (1994) Diurnal regulation of photosynthetic carbon metabolism in C_3 plants. Annu Rev Plant Physiol Plant Mol Biol **45:** 235–256

Gelman A (2006) Prior distributions for variance parameters in hierarchical models (comment on article by Browne and Draper). Bayesian Anal **1:** 515–534

Genty B, Briantais JM, Baker NR (1989) The relationship between the quantum yield of photosynthetic electron transport and quenching of chlorophyll fluorescence. Biochim Biophys Acta **990:** 87–92

Giorio P (2011) Black leaf-clips increased minimum fluorescence emission in clipped leavesexposed to high solar radiation during dark adaptation. Photosynthetica **49:** 371–379

Gómez R, Carrillo N, Morelli MP, Tula S, Shahinnia F, Hajirezaei MR, Lodeyro AF (2018) Faster photosynthetic induction in tobacco by expressing cyanobacterial flavodiiron proteins in chloroplasts. Photosynth Res **136:** 129–138

Govindjee (2002) A role for a light-harvesting antenna complex of photosystem II in photoprotection. Plant Cell **14:** 1663–1668

Grassi G, Magnani F (2005) Stomatal, mesophyll conductance and biochemical limitations to photosynthesis as affected by drought and leaf ontogeny in ash and oak trees. Plant Cell Environ **28:** 834–849

Greenham K, Guadagno CR, Gehan MA, Mockler TC, Weinig C, Ewers BE, McClung CR (2017) Temporal network analysis identifies early physiological and transcriptomic indicators of mild drought in *Brassica rapa*. eLife **6:** e29655

Gu L, Pallardy SG, Tu K, Law BE, Wullschleger SD (2010) Reliable estimation of biochemical parameters from C_3 leaf photosynthesis-intercellular carbon dioxide response curves. Plant Cell Environ **33:** 1852–1874

Gu L, Sun Y (2014) Artefactual responses of mesophyll conductance to CO_2 and irradiance estimated with the variable J and online isotope discrimination methods. Plant Cell Environ **37:** 1231–1249

Guadagno CR, Ewers BE, Speckman HN, Aston TL, Huhn BJ, DeVore SB, Ladwig JT, Strawn RN, Weinig C (2017) Dead or alive? Using membrane failure and chlorophyll *a* fluorescence to predict plant mortality from drought. Plant Physiol **175:** 223–234

Gullì M, Salvatori E, Fusaro L, Pellacani C, Manes F, Marmiroli N (2015) Comparison of drought stress response and gene expression between a GM maize variety and a near-isogenic non-GM variety. PLoS ONE **10:** e0117073

Hammer G, Cooper M, Tardieu F, Welch S, Walsh B, van Eeuwijk F, Chapman S, Podlich D (2006) Models for navigating biological complexity in breeding improved crop plants. Trends Plant Sci **11:** 587–593

Harley PC, Loreto F, Di Marco G, Sharkey TD (1992) Theoretical considerations when estimating the mesophyll conductance to CO_2 flux by analysis of the response of photosynthesis to CO_2. Plant Physiol **98:** 1429–1436

Hill R, Bendall F (1960) Function of the two cytochrome components in chloroplasts: A working hypothesis. Nature **186:** 136–137

Holland JB (2007) Genetic architecture of complex traits in plants. Curr Opin Plant Biol **10:** 156–161

Horton P, Ruban AV, Walters RG (1994) Regulation of light harvesting in green plants (indication by nonphotochemical quenching of chlorophyll fluorescence). Plant Physiol **106:** 415–420

Iniguez-Luy FL, Lukens L, Farnham MW, Amasino RM, Osborn TC (2009) Development of public immortal mapping populations, molecular markers and linkage maps for rapid cycling *Brassica rapa* and *B. oleracea*. Theor Appl Genet **120:** 31–43

Jin Z, Ainsworth EA, Leakey ADB, Lobell DB (2018) Increasing drought and diminishing benefits of elevated carbon dioxide for soybean yields across the US Midwest. Glob Change Biol **24:** e522–e533

Kasahara M, Kagawa T, Oikawa K, Suetsugu N, Miyao M, Wada M (2002) Chloroplast avoidance movement reduces photodamage in plants. Nature **420:** 829–832

Kato MC, Hikosaka K, Hirotsu N, Makino A, Hirose T (2003) The excess light energy that is neither utilized in photosynthesis nor dissipated by photoprotective mechanisms determines the rate of photoinactivation in photosystem II. Plant Cell Physiol **44:** 318–325

Klughammer C, Schreiber U (1994) An improved method, using saturating light pulses, for the determination of photosystem I quantum yield via P700+-absorbance changes at 830 nm. Planta **192:** 261–268

Kramer DM, Avenson TJ, Edwards GE (2004a) Dynamic flexibility in the light reactions of photosynthesis governed by both electron and proton transfer reactions. Trends Plant Sci **9:** 349–357

Kramer DM, Johnson G, Kiirats O, Edwards GE (2004b) New fluorescence parameters for the determination of QA redox state and excitation energy fluxes. Photosynth Res **79:** 209

Krieger-Liszkay A, Fufezan C, Trebst A (2008) Singlet oxygen production in photosystem II and related protection mechanism. Photosynth Res **98:** 551–564

Kruschke JK (2014) Doing Bayesian Data Analysis: A Tutorial with R, JAGS, and Stan. Academic Press, Burlington, MA

Kruschke JK (2018) Rejecting or accepting parameter values in Bayesian estimation, advances in methods and practices. Psychol Sci **1:** 270–280

Kruschke JK, Liddell TM (2018) The Bayesian New Statistics: Hypothesis testing, estimation, meta-analysis, and power analysis from a Bayesian perspective. Psychon Bull Rev **25:** 178–206

Kuhlgert S, Austic G, Zegarac R, Osei-Bonsu I, Hoh D, Chilvers MI, Roth MG, Bi K, TerAvest D, Weebadde P, et al (2016) MultispeQ Beta: A tool for large-scale plant phenotyping connected to the open PhotosynQ network. R Soc Open Sci **3:** 160592

Laisk A, Loreto F (1996) Determining photosynthetic parameters from leaf CO_2 exchange and chlorophyll fluorescence (ribulose-1,5-bisphosphate

carboxylase/oxygenase specificity factor, dark respiration in the light, excitation distribution between photosystems, alternative electron transport rate, and mesophyll diffusion resistance). Plant Physiol **110:** 903–912

Laisk A, Oja V, Rasulov B, Rämma H, Eichelmann H, Kasparova I, Pettai H, Padu E, Vapaavuori E (2002) A computer-operated routine of gas exchange and optical measurements to diagnose photosynthetic apparatus in leaves. Plant Cell Environ **25:** 923–943

Lambrev PH, Miloslavina Y, Jahns P, Holzwarth AR (2012) On the relationship between non-photochemical quenching and photoprotection of photosystem II. Biochim Biophys Acta **1817:** 760–769

Lazár D (2015) Parameters of photosynthetic energy partitioning. J Plant Physiol **175:** 131–147

Li QM, Liu BB, Wu Y, Zou ZR (2008) Interactive effects of drought stresses and elevated CO_2 concentration on photochemistry efficiency of cucumber seedlings. J Integr Plant Biol **50:** 1307–1317

Livingston AK, Cruz JA, Kohzuma K, Dhingra A, Kramer DM (2010) An Arabidopsis mutant with high cyclic electron flow around photosystem I (hcef) involving the NADPH dehydrogenase complex. Plant Cell **22:** 221–233

Long SP, Bernacchi CJ (2003) Gas exchange measurements, what can they tell us about the underlying limitations to photosynthesis? Procedures and sources of error. J Exp Bot **54:** 2393–2401

Malnoë A (2018) Photoinhibition or photoprotection of photosynthesis? Update on the (newly termed) sustained quenching component qH. Environ Exp Bot **154:** 123–133

Martre P, Quilot-Turion B, Luquet D, Memmah MMOS, Chenu K, Debaeke P (2015) Model-assisted phenotyping and ideotype design. *In* VO Sadras, and DF Calderini, eds, Crop Physiology, 2nd ed. Academic Press, London, pp 349–373

Maxwell K, Johnson GN (2000) Chlorophyll fluorescence: A practical guide. J Exp Bot **51:** 659–668

McClain AM, Sharkey TD (2019) Triose phosphate utilization and beyond: From photosynthesis to end product synthesis. J Exp Bot **70:** 1755–1766

McElreath R (2016) Statistical Rethinking: A Bayesian Course with Examples in R and Stan. CRC Press, Boca Raton, FL

Meacham K, Sirault X, Quick WP, von Caemmerer S, Furbank R (2017) Diurnal solar energy conversion and photoprotection in rice canopies. Plant Physiol **173:** 495–508

Medrano H, Escalona JM, Bota J, Gulías J, Flexas J (2002) Regulation of photosynthesis of C3 plants in response to progressive drought: Stomatal conductance as a reference parameter. Ann Bot **89:** 895–905

Miller G, Suzuki N, Ciftci-Yilmaz S, Mittler R (2010) Reactive oxygen species homeostasis and signalling during drought and salinity stresses. Plant Cell Environ **33:** 453–467

Moualeu-Ngangue DP, Chen TW, Stützel H (2017) A new method to estimate photosynthetic parameters through net assimilation rate-intercellular space CO_2 concentration (A-C_i) curve and chlorophyll fluorescence measurements. New Phytol **213:** 1543–1554

Müller P, Li XP, Niyogi KK (2001) Non-photochemical quenching: A response to excess light energy. Plant Physiol **125:** 1558–1566

Murata N, Takahashi S, Nishiyama Y, Allakhverdiev SI (2007) Photoinhibition of photosystem II under environmental stress. Biochim Biophys Acta **1767:** 414–421

Niinemets U, Díaz-Espejo A, Flexas J, Galmés J, Warren CR (2009) Role of mesophyll diffusion conductance in constraining potential photosynthetic productivity in the field. J Exp Bot **60:** 2249–2270

Nishiyama Y, Allakhverdiev SI, Murata N (2006) A new paradigm for the action of reactive oxygen species in the photoinhibition of photosystem II. Biochim Biophys Acta **1757:** 742–749

Noctor G, Veljovic-Jovanovic S, Driscoll S, Novitskaya L, Foyer CH (2002) Drought and oxidative load in the leaves of C3 plants: A predominant role for photorespiration? Ann Bot **89:** 841–850

Nogués S, Baker NR (2000) Effects of drought on photosynthesis in Mediterranean plants grown under enhanced UV-B radiation. J Exp Bot **51:** 1309–1317

Oberhuber W, Edwards GE (1993) Temperature dependence of the linkage of quantum yield of photosystem II to CO_2 fixation in C_4 and C_3 plants. Plant Physiol **101:** 507–512

Ort DR, Baker NR (2002) A photoprotective role for O_2 as an alternative electron sink in photosynthesis? Curr Opin Plant Biol **5:** 193–198

Ort DR, Melis A (2011) Optimizing antenna size to maximize photosynthetic efficiency. Plant Physiol **155:** 79–85

Parry MAJ, Keys AJ, Madgwick PJ, Carmo-Silva AE, Andralojc PJ (2008) Rubisco regulation: A role for inhibitors. J Exp Bot **59:** 1569–1580

Patrick LD, Ogle K, Tissue DT (2009) A hierarchical Bayesian approach for estimation of photosynthetic parameters of C_3 plants. Plant Cell Environ **32:** 1695–1709

Pearcy RW (1990) Sunflecks and photosynthesis in plant canopies. Annu Rev Plant Physiol Plant Mol Biol **41:** 421–453

Pietrini F, Massacci A (1998) Leaf anthocyanin content changes in *Zea mays* L. grown at low temperature: Significance for the relationship between the quantum yield of PS II and the apparent quantum yield of CO_2 assimilation. Photosynth Res **58:** 213–219

Pleban JR, Mackay DS, Aston TL, Ewers BE, Weinig C (2018) Phenotypic trait identification using a multimodel Bayesian method: A case study using photosynthesis in *Brassica rapa* genotypes. Front Plant Sci **9:** 448–468

Plummer M (2003) JAGS: A program for analysis of Bayesian graphical models using Gibbs sampling. https://www.r-project.org/conferences/DSC-2003/Proceedings/Plummer.pdf

Plummer M (2014) rjags: Bayesian graphical models using MCMC. http://mcmc-jags.sourceforge.net/

Pons TL, Flexas J, von Caemmerer S, Evans JR, Genty B, Ribas-Carbo M, Brugnoli E (2009) Estimating mesophyll conductance to CO_2: Methodology, potential errors, and recommendations. J Exp Bot **60:** 2217–2234

Porcar-Castell A, Garcia-Plazaola JI, Nichol CJ, Kolari P, Olascoaga B, Kuusinen N, Fernández-Marín B, Pulkkinen M, Juurola E, Nikinmaa E (2012) Physiology of the seasonal relationship between the photochemical reflectance index and photosynthetic light use efficiency. Oecologia **170:** 313–323

Powles SB (1984) Photoinhibition of photosynthesis induced by visible light. Ann Rev Plant Physiol **35:** 15–44

Prakash S, Hinata K (1980) Taxonomy, cytogenetics and origin of crop *Brassicas*, a review. Opera Bot **55:** 1–57

Rascher U, Bobich E, Lin G, Walter A, Morris T, Naumann M, Nichol C, Pierce D, Bil K, Kudeyarov V (2004) Functional diversity of photosynthesis during drought in a model tropical rainforest: the contributions of leaf area, photosynthetic electron transport and stomatal conductance to reduction in net ecosystem carbon exchange. Plant Cell Environ **27:** 1239–1256

Rascher U, Liebig M, Lüttge U (2000) Evaluation of instant light-response curves of chlorophyll fluorescence parameters obtained with a portable chlorophyll fluorometer on site in the field. Plant Cell Environ **23:** 1397–1405

Reddy AR, Chaitanya KV, Vivekanandan M (2004) Drought-induced responses of photosynthesis and antioxidant metabolism in higher plants. J Plant Physiol **161:** 1189–1202

Reymond M, Muller B, Leonardi A, Charcosset A, Tardieu F (2003) Combining quantitative trait loci analysis and an ecophysiological model to analyze the genetic variability of the responses of maize leaf growth to temperature and water deficit. Plant Physiol **131:** 664–675

Ruban AV (2016) Nonphotochemical chlorophyll fluorescence quenching: Mechanism and effectiveness in protecting plants from photodamage. Plant Physiol **170:** 1903–1916

Sacksteder CA, Kanazawa A, Jacoby ME, Kramer DM (2000) The proton to electron stoichiometry of steady-state photosynthesis in living plants: A proton-pumping Q cycle is continuously engaged. Proc Natl Acad Sci USA **97:** 14283–14288

Sharkey TD, Bernacchi CJ, Farquhar GD, Singsaas EL (2007) Fitting photosynthetic carbon dioxide response curves for C_3 leaves. Plant Cell Environ **30:** 1035–1040

Sharma P, Jha AB, Dubey RS, Pessarakli M (2012) Reactive oxygen species, oxidative damage, and antioxidative defense mechanism in plants under stressful conditions. J Bot **2012:** 217037

Sheffield J, Wood EF (2008) Projected changes in drought occurrence under future global warming from multi-model, multi-scenario, IPCC AR4 simulations. Clim Dyn **31:** 79–105

Shi J, Li R, Qiu D, Jiang C, Long Y, Morgan C, Bancroft I, Zhao J, Meng J (2009) Unraveling the complex trait of crop yield with quantitative trait loci mapping in *Brassica napus*. Genetics **182:** 851–861

Silva-Perez V, Molero G, Serbin SP, Condon AG, Reynolds MP, Furbank RT, Evans JR (2018) Hyperspectral reflectance as a tool to measure biochemical and physiological traits in wheat. J Exp Bot **69:** 483–496

Singsaas EL, Ort DR, DeLucia EH (2001) Variation in measured values of photosynthetic quantum yield in ecophysiological studies. Oecologia **128:** 15–23

Souza RP, Machado EC, Silva JAB, Lagôa AMMA, Silveira JAG (2004) Photosynthetic gas exchange, chlorophyll fluorescence and some associated metabolic changes in cowpea (*Vigna unguiculata*) during water stress and recovery. Environ Exp Bot **51:** 45–56

Strand DD, Livingston AK, Satoh-Cruz M, Froehlich JE, Maurino VG, Kramer DM (2015) Activation of cyclic electron flow by hydrogen peroxide in vivo. Proc Natl Acad Sci USA **112:** 5539–5544

Takahashi S, Badger MR (2011) Photoprotection in plants: A new light on photosystem II damage. Trends Plant Sci **16:** 53–60

Tardieu F (2003) Virtual plants: Modelling as a tool for the genomics of tolerance to water deficit. Trends Plant Sci **8:** 9–14

Tazoe Y, von Caemmerer S, Badger MR, Evans JR (2009) Light and CO_2 do not affect the mesophyll conductance to CO_2 diffusion in wheat leaves. J Exp Bot **60:** 2291–2301

Tietz S, Hall CC, Cruz JA, Kramer DM (2017) NPQ_T: A chlorophyll fluorescence parameter for rapid estimation and imaging of non-photochemical quenching of excitons in photosystem-II-associated antenna complexes. Plant Cell Environ **40:** 1243–1255

Urban L, Aarrouf J, Bidel LPR (2017) Assessing the effects of water deficit on photosynthesis using parameters derived from measurements of leaf gas exchange and of chlorophyll *a* fluorescence. Front Plant Sci **8:** 2068

Vialet-Chabrand S, Matthews JSA, Brendel O, Blatt M, Wang Y, Hills A, Griffiths H, Rogers S, Lawson T (2016) Modelling water use efficiency in a dynamic environment: An example using *Arabidopsis thaliana*. Plant Sci **251:** 65–74

Vialet-Chabrand S, Matthews JSA, Simkin AJ, Raines CA, Lawson T (2017) Importance of fluctuations in light on plant photosynthetic acclimation. Plant Physiol **173:** 2163–2179

Von Caemmerer S (2000) Biochemical Models of Leaf Photosynthesis. CSIRO Publishing, Collingwood, Victoria, Australia

Wang DR, Guadagno CR, Mao X, Mackay DS, Pleban JR, Baker RL, Weinig C, Jannink JL, Ewers BE (2019) A framework for genomics-informed ecophysiological modeling in plants. J Exp Bot **70:** 2561–2574

Way DA, Pearcy RW (2012) Sunflecks in trees and forests: From photosynthetic physiology to global change biology. Tree Physiol **32:** 1066–1081

Williams PH, Hill CB (1986) Rapid-cycling populations of Brassica. Science **232:** 1385–1389

Yarkhunova Y, Edwards CE, Ewers BE, Baker RL, Aston TL, McClung CR, Lou P, Weinig C (2016) Selection during crop diversification involves correlated evolution of the circadian clock and ecophysiological traits in *Brassica rapa*. New Phytol **210:** 133–144

Yin X, Harbinson J, Struik PC (2006) Mathematical review of literature to assess alternative electron transports and interphotosystem excitation partitioning of steady-state C3 photosynthesis under limiting light. Plant Cell Environ **29:** 1771–1782

Yin X, Struik PC, Romero P, Harbinson J, Evers JB, van der Putten PE, Vos J (2009) Using combined measurements of gas exchange and chlorophyll fluorescence to estimate parameters of a biochemical C photosynthesis model: A critical appraisal and a new integrated approach applied to leaves in a wheat (*Triticum aestivum*) canopy. Plant Cell Environ **32:** 448–464

Yin X, Van Oijen M, Schapendonk A (2004) Extension of a biochemical model for the generalized stoichiometry of electron transport limited C3 photosynthesis. Plant Cell Environ **27:** 1211–1222

Zavafer A, Cheah MH, Hillier W, Chow WS, Takahashi S (2015) Photodamage to the oxygen evolving complex of photosystem II by visible light. Sci Rep **5:** 16363